Biosensors and Bioelectronics 89 (2017) 56–71

Contents lists available at ScienceDirect

Biosensors and Bioelectronics

journal homepage: www.elsevier.com/locate/bios

# Two-dimensional $MoS_2$: A promising building block for biosensors

Xiaorong Gan, Huimin Zhao *, Xie Quan

*Key Laboratory of Industrial Ecology and Environmental Engineering (Ministry of Education, China), School of Environmental Science and Technology, Dalian University of Technology, Dalian 116024, China*

ARTICLE INFO

*Article history:*
Received 29 November 2015
Received in revised form
27 February 2016
Accepted 17 March 2016
Available online 22 March 2016

*Keywords:*
Two-dimensional nanomaterials
$MoS_2$
Biosensors

ABSTRACT

Recently, two-dimensional (2D) layered nanomaterials have trigged intensive interest due to the intriguing physicochemical properties that stem from a quantum size effect connected with their ultra-thin structure. In particular, 2D molybdenum disulfide ($MoS_2$), as an emerging class of stable inorganic graphene analogs with intrinsic finite bandgap, would possibly complement or even surpass graphene in electronics and optoelectronics fields. In this review, we first discuss the historical development of ultrathin 2D nanomaterials. Then, we are concerned with 2D $MoS_2$ including its structure–property relationships, synthesis methods, characterization for the layer thickness, and biosensor applications over the past five years. Thereinto, we are highlighting recent advances in 2D $MoS_2$-based biosensors, especially emphasize the preparation of sensing elements, roles of 2D $MoS_2$, and assay strategies. Finally, on the basis of the current achievements on 2D $MoS_2$ and other ultrathin layered nanomaterials, perspectives on the challenges and opportunities for the exploration of 2D $MoS_2$-based biosensors are put forward.



**Contents**



## 1. Introduction

Two dimensional (2D) layered nanomaterials are an emerging but important class of materials. Strictly speaking, they refer to the layers materials with one dimension restricted to a single-atom layer, while in literatures they include monolayer and few-layer nanomaterials (Gupta et al., 2015; Naguib and Gogotsi, 2015; Tan and Zhang, 2015; Tang and Zhou, 2013; Zhang, 2015). According to the morphology and thickness, they could be divided into nanoribbons, nanoplates, nanowalls, and nanoflakes or nanosheets (Zhou et al., 2013), in which the lateral dimensions are one or

* Corresponding author.
*E-mail address:* zhaohuim@dlut.edu.cn (H. Zhao).

http://dx.doi.org/10.1016/j.bios.2016.03.042
0956-5663/

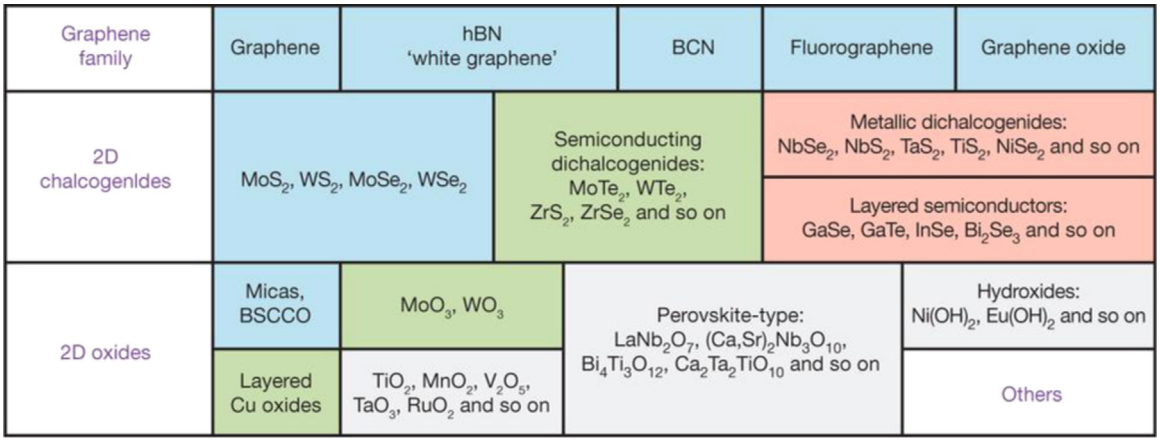


**Fig. 1.** Current 2D library. Monolayers proved to be stable under ambient conditions (room temperature in air) are shaded blue; those probably stable in air are shaded green; and those unstable in air but that may be stable in inert atmosphere are shaded pink. Gray shading indicates 3D compounds that have been successfully exfoliated down to monolayers, as is clear from atomic force microscopy, for example, but for which there is little further information. Reproduced from (Geim and Grigorieva, 2013) with permission from Nature Publishing Group. (For interpretation of the references to color in this figure legend, the reader is referred to the web version of this article.)

several orders of magnitude larger than the thickness. They are usually but not necessarily prepared by exfoliating their bulk counterparts that have weak interaction between the neighboring layers (Pan et al., 2014).

In addition to the composition and atomic arrangement, dimensionality plays a critical role in determining the fundamental properties of 2D nanomaterials (Chhowalla et al., 2013). Due to the quantum effects, 2D nanomaterials exhibit unique physical and chemical properties that differ from their bulk counterparts. So far, the potential applications in electronics, optoelectronics, sensors, catalysis, gas separation, energy storage and conversion, water remediation, and biomedicine, have demonstrated the versatility of 2D nanomaterials (Kannan et al., 2015; Sun et al., 2015; Zhang, 2015). The known 2D nanomaterials mainly include graphene, graphitic carbon nitride (g-$C_3N_4$), hexagonal boron nitride (hBN), transition metal dichalcogenides (TMDCs), metal oxides and hydroxides (including clays), black phosphorene, group IV elements (*i.e.,* silicene, germanene, and stanene, *etc.*), metalorganic frameworks (MOFs), covalent-organic frameworks (COFs), polymers, and metals (Colson et al., 2011; Houssa et al., 2015; Huang et al., 2011, 2013c; Jiang et al., 2015; Kaul, 2014; Kory et al., 2014; Kou et al., 2015; Peng et al., 2014; Zhuang et al., 2015).

Even though the initial studies about layered materials can date back to molybdenum disulfide ($MoS_2$) in the 1970s (Pisoni et al., 2015), the burgeoning research on 2D nanomaterials really began after graphene was discovered in 2004 (Novoselov et al., 2004). The impressive advancements of graphene in a wide range of fields have triggered the strong research interest in the broader family "beyond graphene" that would offer greater choices to be explored and tailored for various applications (Kuc and Heine, 2015). In particular, 2D layered TMDCs exhibit a wealthy of fascinating properties that depend on their composition and layer thickness ranging from semiconductors and semimetals to true metals and superconductors (Ganatra and Zhang, 2014; Heine, 2015; Wang et al., 2012). The process or conversion could be realized by modifying the electron filling by doping, quantum size effect, field effect, or intercalation of molecules, atoms, and ions into van der Waals layers (Cha et al., 2013). Most hopefully, 2D $MoS_2$, as one of stable layered TMDCs (Fig. 1), demonstrates unique electronic, optical, mechanical, and chemical characteristics (Ataca et al., 2012; Geim and Grigorieva, 2013; Huang et al., 2014f). It will complement or even surpass graphene (zero band gap) in electronics and optoelectronics fields, such as field effect transistors (FETs), phototransistors, logic circuits, due to its intrinsic finite bandgap, high on/off ratio, and abundance of bulk material (Butler et al., 2013; Lee et al., 2010; Li and Zhu, 2015; Radisavljevic et al., 2011; Su et al., 2015). Most importantly, its ultrathin plane structure where the electrons/holes are confined to a plane of atomic thickness makes 2D $MoS_2$ sensitive to the surrounding environment (Chen et al., 2009); therefore, to large extent, 2D $MoS_2$ would be a promising building block for biosensors (Kalantar-zadeh and Ou, 2016; Zhang et al., 2015c).

Herein, we give a brief overview of progress on 2D $MoS_2$ rather than offering a comprehensive review. In the following sections, we first discuss the relationship between structure and property/function, mainly about the changes of its bandgap structure with the thickness that is responsible for the electronics and optoelectronics properties. Later on, we summarize the typical synthetic methods, including the pros and cons for specific biosensors. Further, we discuss several simple but effective analytical methods including Raman spectroscopy, optical extinction spectroscopy, photoluminescence spectroscopy for characterizing its layer thickness. In addition, we highlight its biosensing applications including electrochemical biosensors, fluorescent biosensors, colorimetric biosensors, electrochemiluminescence biosensors, and field effect transistor biosensors for the last few years, as shown in Fig. 2. Finally, we provide some personal opinions on the development direction and challenge of 2D $MoS_2$-based biosensors. Due to the explosion of publications in this active field and limited by our knowledge, we do not claim that this review includes all of the published works in the past.

## 2. Structure–property relationships of 2D $MoS_2$

In general, material properties are associated with their electronic structures, especially the position of Fermi level and the size and shape of Fermi surfaces (Zhao et al., 2015). In detail, for 2D $MoS_2$, the structure and layer number as well as layer–substrate interaction could greatly affect its physical and chemical properties (Robinson et al., 2015). In essence, they all belong to band engineering for tailoring the properties of 2D $MoS_2$ (Guo et al., 2015; Zeng et al., 2015b). In the following section, the structure–property relationship of $MoS_2$ would be discussed mainly according to its electron energy band structure.

2D $MoS_2$ or $MoS_2$ has three polytypic structures including 2H (trigonal prismatic coordination), 1T (octahedral crystal symmetry configuration), and 1T' (distorted 1T), as shown in Fig. 3A. Thereinto, 2H-and 1T-$MoS_2$ phases are most extensively studied in both theory calculations and experiments in recent years (Gao et al.,

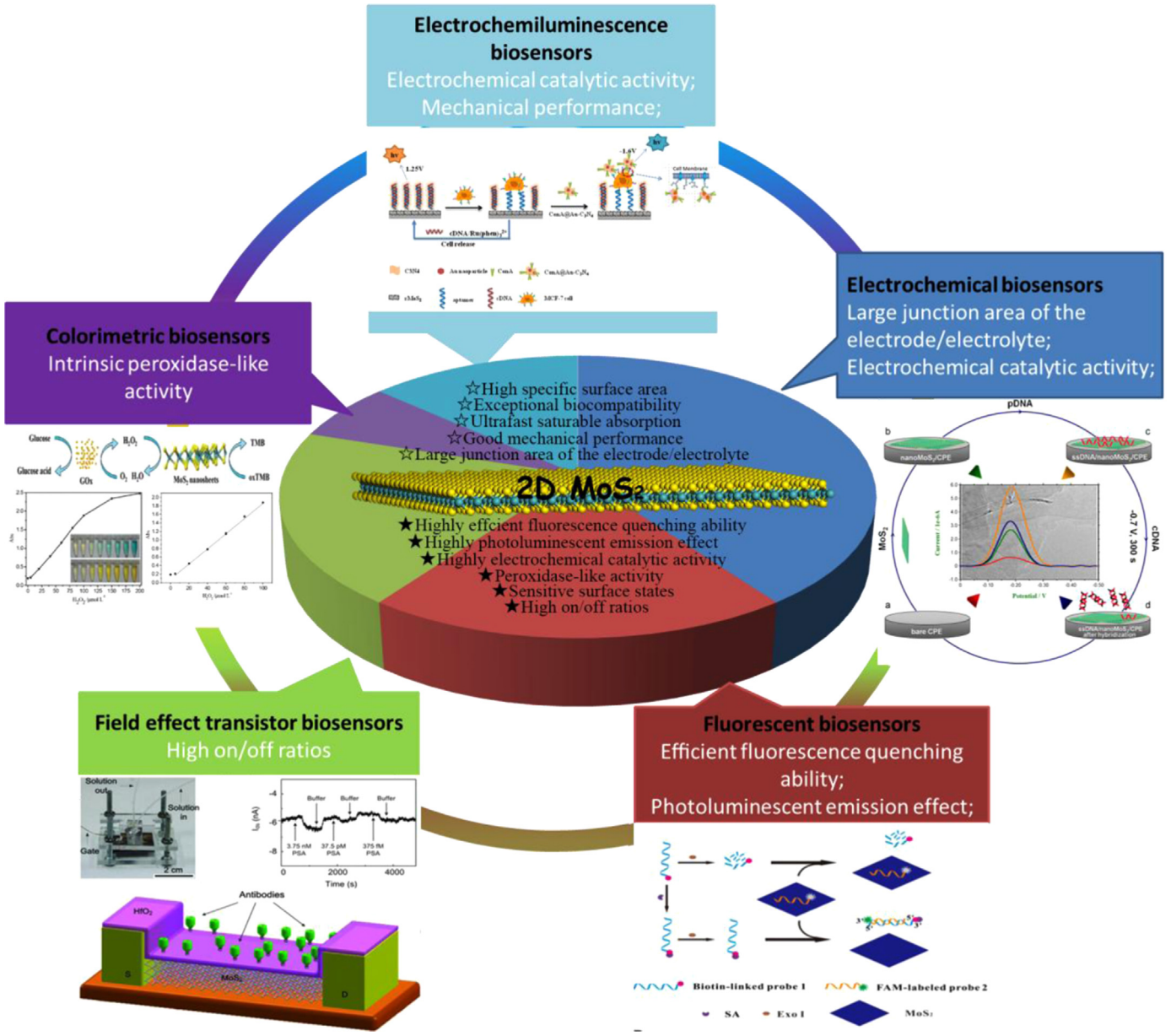


**Fig. 2.** Intrinsic properties of 2D $MoS_2$ and most representative properties applied in a specific biosensor. Here, the distribution proportion in pie chart was obtained after the statistical analysis of references in the review.

2015). In 2H-$MoS_2$ coordination, the d orbitals split into three bands, namely, $d_{z^2}$,$d_{x^2-y^2,xy}$, and $d_{xz,yz}$, separated by an energy gap. The orbitals are located within the bonding ($\sigma$) and antibonding ($\sigma^*$) states. In 1T coordination, the d orbitals split into $d_{xz,yz,zx}$ and $d_{z^2,x^2-y^2}$. The partially filled $d_{xz,yz,zx}$ orbital in the 1T phase leads to metallic in electronic character, while in the 2H phase the two d electrons of $d_{z^2}$ orbital, makes it a semiconductor. 1T-$MoS_2$ phase is unstable under ambient condition, and readily transforms back to the thermodynamically stable 2H phase or 1T' phase. Under certain conditions, the phase conversion could occur between prototypes of $MoS_2$, such as 2H-$MoS_2$→1T-$MoS_2$ and 2H-$MoS_2$→1T'-$MoS_2$.

Even though $MoS_2$ was the first investigated in 2D nanomaterials (Del Corro et al., 2014), it is paid with extensive attention after the advent of isolated 2D $MoS_2$. In particular monolayer $MoS_2$ exhibits many unique properties due to a quantum size effect connected with its ultra-thin structure (Jia et al., 2015; Zeng et al., 2011). Monolayer $MoS_2$, 6.5 Å thick, is centrosymmetric and composed of three atom layers, namely, a Mo layer sandwiched between two S layers. It could be particularly stable even in liquid and oxygen containing gaseous media due to no dangling bonds at the end of basal surfaces (Kalantar-Zadeh and Ou, 2016). As for few-layer $MoS_2$, its special bond structure, strong molecular intralayer bonds (coordination bonds) but weak interlayer bonds, leads to the highly anisotropic properties that mechanical, thermal, and electrical properties in plane are significantly different with those out of plane (Chia et al., 2015).

In addition, the lack of inversion symmetry, confinement of electron motion in plane, and high mass of the elements cause a very strong spin-orbit splitting for applications in spin-based or valley-based electronics (Vogel and Robinson, 2015). From bulk to monolayer $MoS_2$, its band gap could change from 1.2 to 1.9 eV. Moreover, its bandgap exhibits an indirect-to-direct transition (Fig. 3B) which leads to the strong photoluminescence emission (Kuc et al., 2011). In terms of the direct bandgap, the valence band maximum and the conduction band minimum are both located at

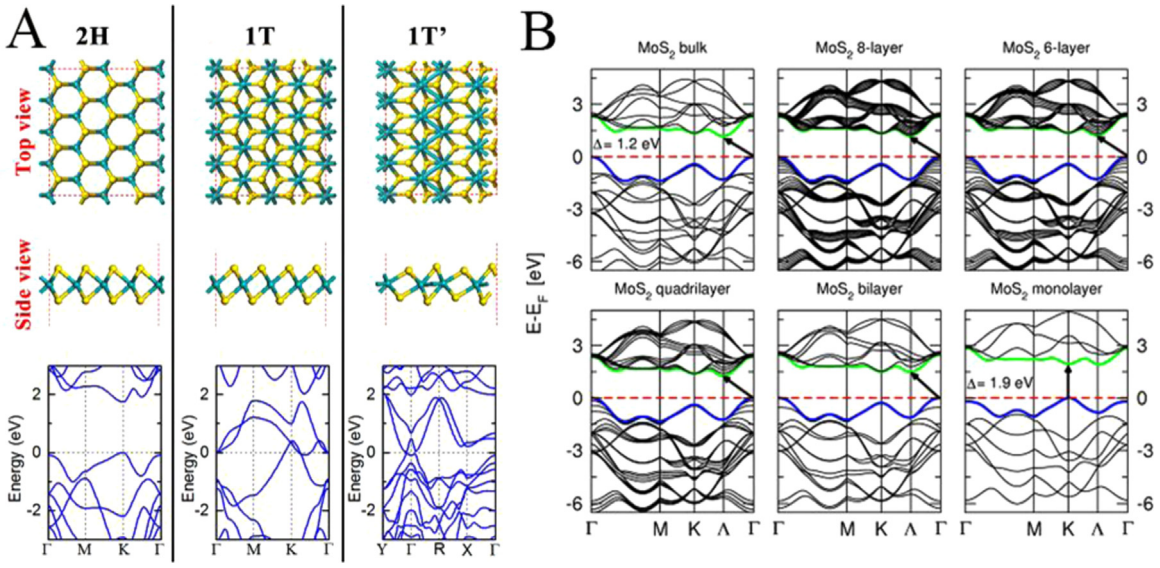


**Fig. 3.** (A) Top view and side view of 2H, 1T, and 1T' $4 \times 4 \times 1$ $MoS_2$ and their band structures. Cyan, Mo; yellow, S. Reproduced from Gao et al. (2015) with permission from American Chemical Society. (B) Band structure of $MoS_2$ in bulk, multilayer, bilayer, and monolayer forms. Reproduced from Kuc et al. (2011) with permission from American Physical Society. (For interpretation of the references to color in this figure legend, the reader is referred to the web version of this article.)

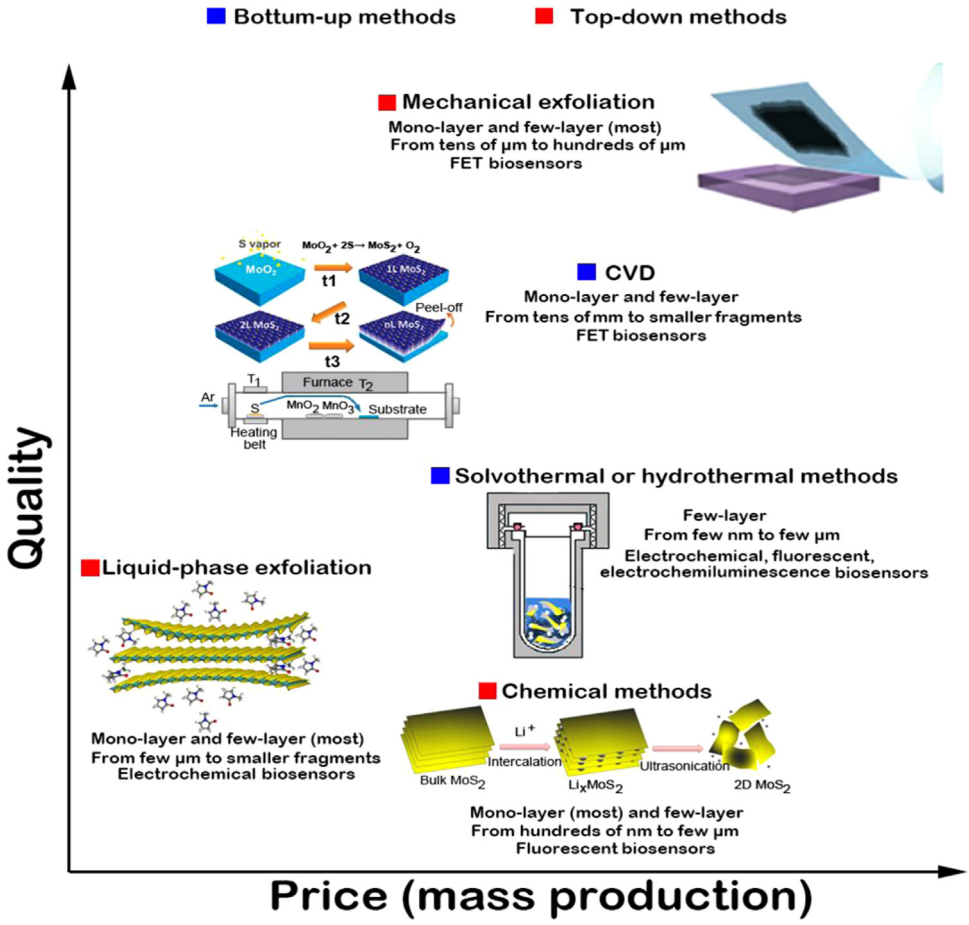


**Fig. 4.** Several synthesis methods of mass-production of 2D $MoS_2$, their characteristic size and thickness distributions of the resultant 2D $MoS_2$, and correspondingly typical biosensor application. Partly reproduced from Novoselov et al. (2012) with permission from Nature Publishing Group.

the K point (Gołasa et al., 2014). Its layer-dependent band structure is ascribed to quantum confinement and the resulting changes in hybridization between $p_z$ orbitals on S atoms and d orbitals on Mo atoms (Mak et al., 2010).

At room temperature, compared with bulk $MoS_2$, the charge carrier mobility of monolayer $MoS_2$ is sharply decreased due to the phonon-scattering, in the range 0.1–10 $cm^2 V^{-1} s^{-1}$ (Radisavljevic and Kis, 2013). On the other hand, charge traps at the interface between the substrate and 2D $MoS_2$ is the dominant cause for such low room-temperature mobility of $MoS_2$ devices (Ghatak et al., 2011).

Interestingly, the "sandwich" structure synthesized by the deposition of a high-K dielectric material on the surface of 2D $MoS_2$ could significantly improve the mobility via suppression of Coulomb scattering (Yoon et al., 2011). By dielectric screening, at room-temperature the charge carrier mobility of single-layer $MoS_2$ could at least reach 200 $cm^2 V^{-1} s^{-1}$, which is extensively used to improve the performances of 2D $MoS_2$-based field-effect transistors (FETs) biosensors (Radisavljevic and Kis, 2013; Radisavljevic et al., 2011).

## 3. Synthesis methods of 2D $MoS_2$

Different synthesis methods will dramatically affect the properties of as-obtained 2D $MoS_2$ and thus its biosensing applications (Fig. 4). Therefore, it is necessary to discuss the synthesis methods. Thanks to the advancements in graphene research, various synthesis methods have been established which enabled the field of 2D materials beyond graphene to mature very quickly. In general, the synthesis methodologies for 2D $MoS_2$ could be divided into two categories: top-down and bottom-up methods (Najmaei et al., 2015).

Thereinto, bottom-up methods include chemical vapor deposition (CVD) and solvothermal or hydrothermal methods (Perumal Veeramalai et al., 2015). The CVD technique is advantageous for preparing high-quality 2D $MoS_2$ with a scalable size, controllable thickness, and excellent electronic properties (Shi et al., 2015c). A typical procedure is that different solid precursors, such as sulfur powder and $MoO_3$ powder, are vaporized in reduction (e.g., $H_2$) or inert (e.g., Ar) atmosphere by the heart resources, such as the electron, laser, and plasma beams (Castellanos-Gomez et al., 2012; Choudhary et al., 2014; Liu et al., 2013; Mahjouri-Samani et al., 2015), and then co-deposited onto a nearby substrate ($SiO_2$ (Zhang et al., 2014a), mica (Ji et al., 2013), $SrTiO_3$ (Zhang et al., 2014b), Au foil (Shi et al., 2015b), and graphene (McCreary et al., 2014; Shi et al., 2012)). A challenge of the method is how to achieve the simple, highly efficient, and control growth of ultrathin 2D $MoS_2$ nanomaterials on arbitrary substrates at low temperature, meanwhile to avoid the complicated transfer process. Because of its large size on the order of tens of millimeters (Lv et al., 2015), and high crystal quality, 2D $MoS_2$ prepared by CVD is usually used in constructing FET biosensors.

Solvothermal or hydrothermal methods are simple, scalable, and readily controlled (Prabhakar Vattikuti et al., 2015); however, they usually consume more energy and require high temperature and pressure, and special organic reagents for solubilizing precursors, which can be aggressive to the equipment and sensitive to the environmental conditions (Wang et al., 2013c). In generally, the parameters for control synthesis include precursors, pH value, pressure, time, and temperature (Wang et al., 2015b). Thereinto, low pH value and pressure are beneficial for obtaining 2D $MoS_2$ with a higher specific surface area. Nevertheless, the morphology tends to be a hierarchical structure such as 3D flower-like (Veeramalai et al., 2015). Compared with CVD, an obvious advantage of this technique is easily to obtain much smaller crystallites with highly catalytic activity which have a great potential in constructing electrochemical, fluorescent, electrochemiluminescence biosensors. The most significant challenges of such technique lie in the availability and selection of appropriate metal and chalcogen reagents, control over metal oxidation states, achieving high purity and yield, and understanding how to truncate vertical growth while permitting lateral growth (Jeong et al., 2012).

Top-down methods mainly include mechanical exfoliation, chemical or electrochemical exfoliation methods, and liquid-phase exfoliation. The mechanical exfoliation is derived from "scotch tape" method for graphene (Novoselov et al., 2005; Ramakrishna Matte et al., 2010). In the process, a small high-quality bulk $MoS_2$ crystal is adhered to a stretch of adhesive tape, repeatedly exfoliated followed by being adhered on a substrate. This causes ultrathin material layers to be left on the substrate. The method can produce single-crystal flakes of high purity, big size, and cleanliness that are most suitable for understanding the physical and chemical properties of 2D $MoS_2$ and building 2D $MoS_2$-based field-effect transistor-based biosensors. However, it is hard to realized scalable production and systematic control of flake thickness, shape, and size.

Chemical methods, generally based on ion intercalation (e.g., $SO_4^{2-}$ and $Li^+$) (Liu et al 2014b; Niu and Li, 2015), are relatively time-consuming but high yielding in monolayer $MoS_2$. For instance, the $Li^+$-intercalation and exfoliation method involves harsh chemical treatments that must be carried out in an inert atmosphere. In addition, it readily results in defects and structural deformations that would considerably alter electronic properties of 2D $MoS_2$ (Sandoval et al., 1991). Therefore, this method is not proper for investigating the physical or chemical properties of 2D $MoS_2$. However, it is advantageous for high efficiency of producing single-layer $MoS_2$ for constructing fluorescent biosensors.

Recently, liquid phase exfoliation (LPE), also called sonication-assisted exfoliation in solvents or aqueous surfactant solutions (Radisavljevic et al., 2011), is the most suitable route for large scale production of 2D $MoS_2$ (Nicolosi et al., 2013; Yu et al., 2015), due to simplicity and lack of a third-phase dispersant (e.g., a surfactant solution) (Cunningham et al., 2012). The technique is frequently used in electrochemical biosensors due to its high electrochemical catalytic activity and electron transfer capacity (Wang et al., 2015d). Furthermore, 2D $MoS_2$ obtained by this method allows the formation of films and the production of hybrids and composites for additional applications (Coleman et al., 2011; Smith et al., 2011). If a proper solution could be chosen, this method would be applicable to any layered materials held together by the relatively weak van der Waals bonds. Moreover, it could result in high quality, relatively high throughput, and stabilized preservation of 2D $MoS_2$ (Backes et al., 2014). In general, the proper solvent must fulfill the following two criteria: firstly it must be able to vigorously exfoliate bulk $MoS_2$ at the highest concentration as much as possible; secondly, it could make the obtained 2D $MoS_2$ stable for the longest duration. In detail, the solvent has a feature not only in a surface energy (or surface tension), equal or close, as much as possible, with that of bulk counterparts, but also in the ratio of polar ($\sigma_p$) and dispersive ($\sigma_d$) contributions of interfacial surface tension (Shen et al., 2015). Therefore, N, N-dimethylformamide (DMF) is, in theoretical, the best solvent for preparing 2D $MoS_2$.

## 4. Characteristic methods for 2D $MoS_2$ thickness

Because the physical and chemical properties of 2D $MoS_2$ are strongly dependent on the layer thickness (Lu et al., 2012), how to locate and identify the mono- and multi-layer 2D $MoS_2$ in a rapid and accurate way is the first step prior to the fundamental research and practical applications. Here our emphasis would focus on some straightforward but effective characteristic methods for probing the layer thickness, which include Raman spectroscopy, optical extinction spectroscopy (absorption spectroscopy), and photoluminescence spectroscopy.

### 4.1. Raman spectroscopy

Raman spectroscopy is an excellent tool to unambiguously pinpoint the number of sheets of the layered TDM materials due to its simplicity and ability to provide nondestructive structural information about nanomaterials (Chakraborty et al., 2013; Chen et al., 2015a; Pimenta et al., 2015; Tonndorf et al., 2013). Until now, most research work focused on the intra-layer vibrations with

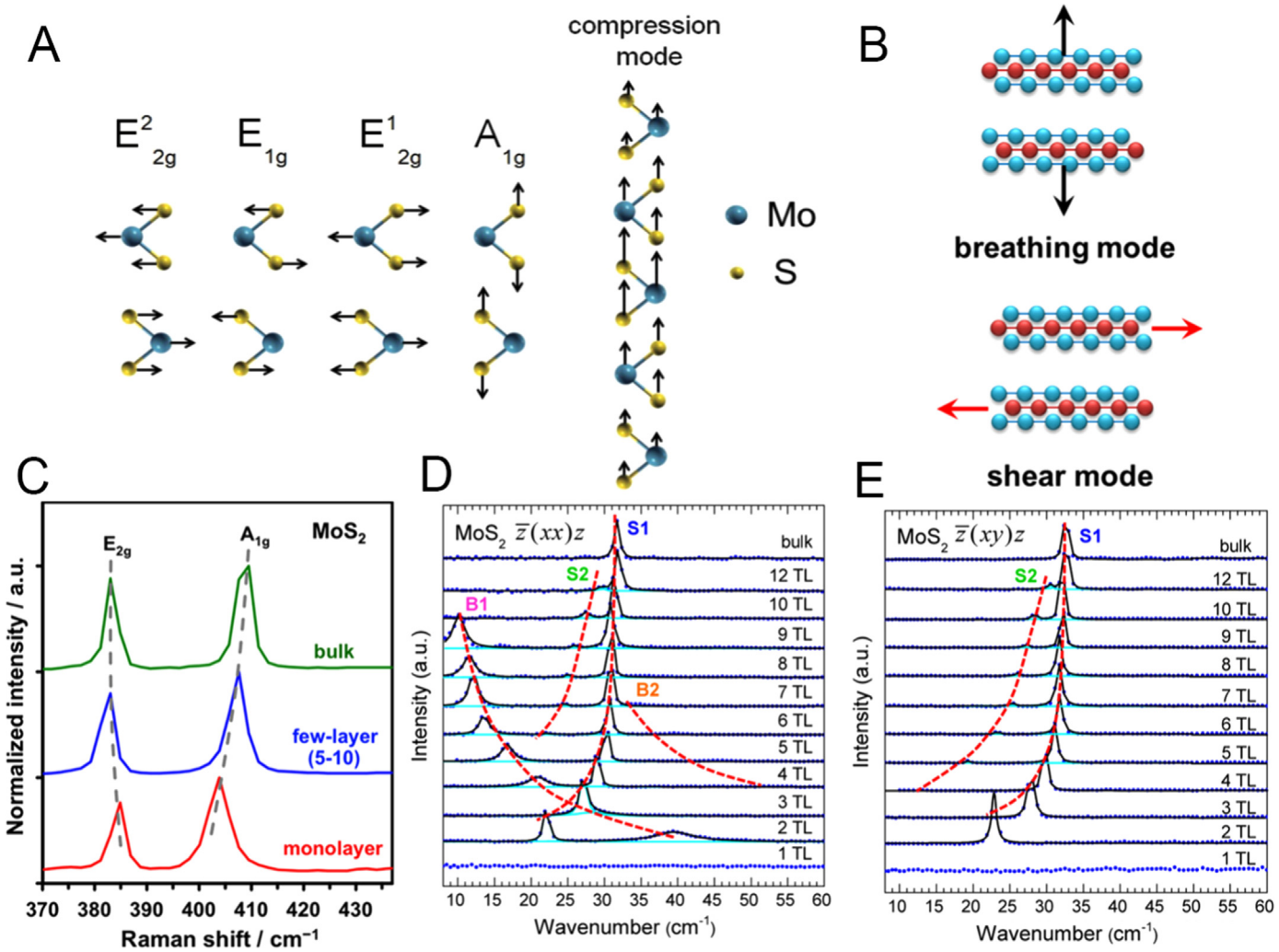


**Fig. 5.** (A) Illustrations of the four Raman-active phonon modes and their interlayer interactions. (B) Illustrations of the interlayer breathing and shear modes. (C) $E_{2g}{}^1$ and $A_{1g}$ Raman peaks in monolayer/few-layer/bulk $MoS_2$. (D and E) Evolution of low-frequency spectra with increasing layer number of the interlayer breathing (B1 and B2) and shear (S1 and S2) modes using (D) the $(xx)_z$ polarization configuration and (E) the $(xy)_z$ polarization configuration. Panel A reproduced from Zeng et al. (2012) with permission from American Chemical Society. Panel C reproduced from Velicky et al. (2016) with permission from American Chemical Society. Panels B, D, and E reproduced from Zhao et al. (2013) with permission from American Chemical Society.

relatively large frequencies $>100\ cm^{-1}$, even though Raman spectral frequencies below $\sim 50\ cm^{-1}$ also contains a wealth of information. Especially, some low-frequency (LF) modes, such as shear and breathing modes (Fig. 5B), could provide the most sensitive measurements of the van der Waals interactions and coupling between layers in stacked 2D crystals with different numbers of layers and phases (Zeng et al., 2012). Therefore, they can be used to deterministically identify the layer number of 2D $MoS_2$.

Because the 1T phase of $MoS_2$ is metastable, we would focus the discussion only on the Raman spectrum of 2H-$MoS_2$. Generally, it has four Raman-active modes of $A_{1g}$, $E_{1g}$, $E_{2g}{}^1$, and $E_{2g}{}^2$ (Fig. 5A) with wavenumbers approximately at $408\ cm^{-1}$, $286\ cm^{-1}$, $383\ cm^{-1}$, and $32\ cm^{-1}$, respectively (Li et al., 2012b). The four Raman-active modes are assigned accordingly to the representations of the $D_{6h}$ group (Chakraborty et al., 2013). Thereinto, the $E_{1g}$ mode is hardly observed due to the forbidden selection rule in the backscattering geometry. It involves in-plane (S–Mo–S) atomic vibrations, the opposite vibration of two S atoms with respect to the Mo atom between them. The $A_{1g}$ mode is attributed to the out-of-plane vibration of only S atoms in opposite directions. With increasing number of layers, theoretically both $A_{1g}$ mode and $E_{2g}{}^1$ mode would exhibit a blue-shift because the interlayer van der Waals force could suppress atom vibration and result in higher force constants; however, a redshift occurs for the $E_{2g}{}^1$ mode while a blueshift is for the $A_{1g}$ mode (Fig. 5C) (Zeng et al., 2012). This phenomenon is ascribed to an enhancement of the dielectric screening of the long-range Coulomb interaction between the effective charges with a growing number of layers (Molina-Sánchez and Wirtz, 2011). Taken together, this implies that the increased interlayer van der Waals force plays a minor role, while stacking-induced structure changes or long-range Coulombic interlayer interactions in multilayer $MoS_2$ may dominate the changes of atomic vibration (Lee et al., 2010). In general, the frequency or frequency-shift difference between $A_{1g}$ and $E_{2g}{}^1$ modes can be used to determine the layer number of few-layer $MoS_2$ nanosheets or flakes, excepting 2D $MoS_2$ synthesized by LPE (Guan et al., 2015) or chemical methods (e.g., Li-intercalated and exfoliation) (Yang et al., 1991). The possible reason is that the $A_{1g}$ mode is less affected by interlayer interactions, but very sensitive to electron doping and adsorbates on the surface of $MoS_2$ (Chakraborty et al., 2012; Perkins et al., 2013). Because of stronger electron–phonon coupling, the $A_{1g}$ mode undergoes a redshift and an increase in the peak width with increasing doping level. In addition, surface reconstruction could to some extent result in the shift of $E_{2g}{}^1$ and $A_{1g}$ modes.

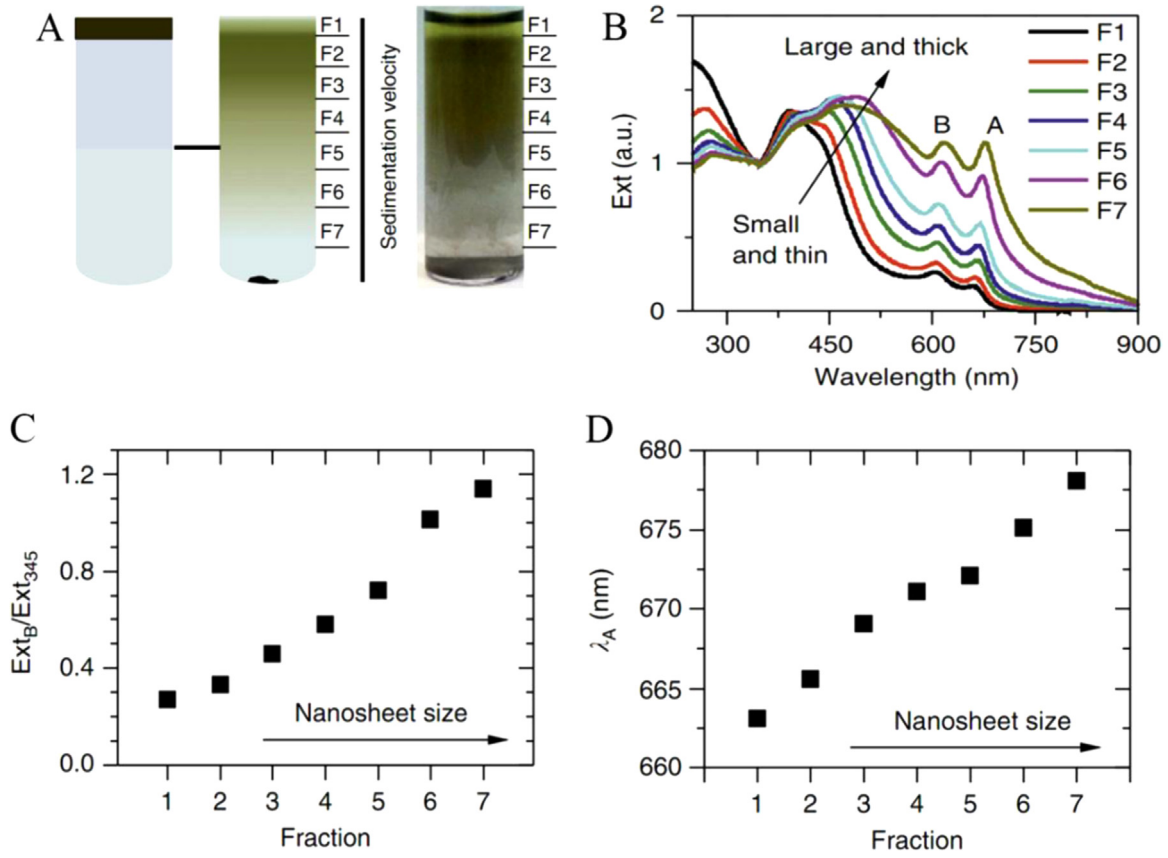


**Fig. 6.** $MoS_2$ band sedimentation and size-dependent extinction spectra. (A) Experimental setup for band sedimentation centrifugation involving layering a nanomaterial stock dispersion on top of a race layer. (B) Extinction spectra of the fractions normalized to the local minimum at 345 nm. The positions of the A-and B-excitons are marked. (C) Ratio of extinction at B-exciton to that at 345 nm, $Ext_B/Ext_{345}$ plotted versus fraction number. (D) Peak position (wavelength) of the A-exciton, $\lambda_A$, as a function of fraction number. Reproduced from Backes et al. (2014) with permission from Nature Publishing Group.

Low-frequency interlayer breathing ($B_{2g}{}^2$) and shear ($E_{2g}{}^2$) modes (see Fig. 5B, D and E) are associated with in-plane and out-of-plane interlayer vibrations, respectively. With increasing number of layers, the $E_{2g}{}^2$ mode shows a blueshift, while the opposite is observed for the $B_{2g}{}^2$ mode. Both modes vanish for single-layer $MoS_2$, being consistent with the understanding that these two modes are a result of interlayer interaction. In addition, the distance between the in-plane $E_{2g}{}^1$ mode and out-of-plane $A_{1g}$ mode could also be used to qualitatively determine monolayer $MoS_2$ or not (Liu et al., 2014a).

### 4.2. Optical extinction spectroscopy

As mentioned above, Raman spectrum could not provide the accurate information about its thickness of 2D $MoS_2$ prepared by LPE or chemical method. Recent research has demonstrated that optical

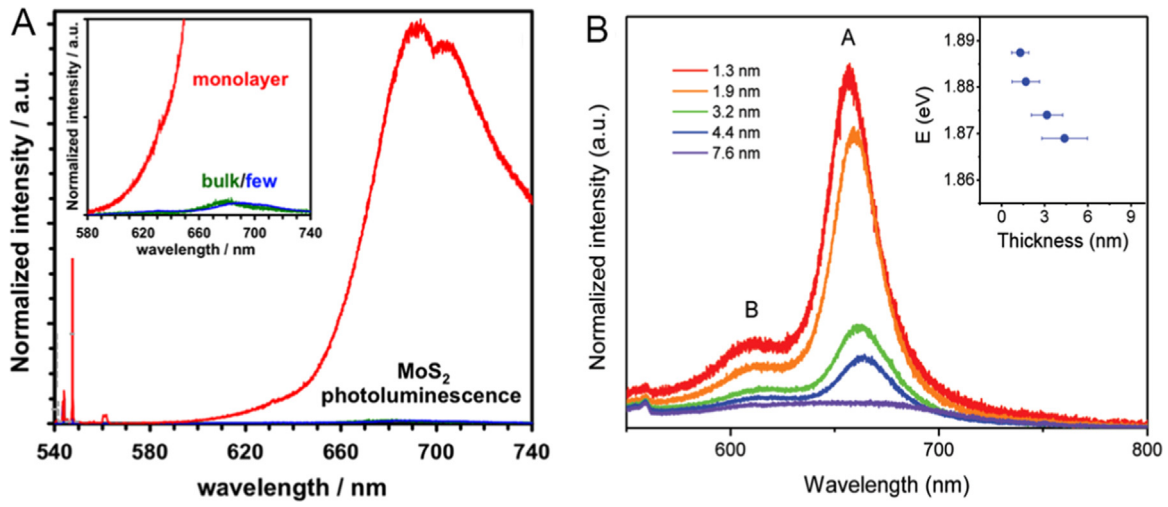


**Fig. 7.** Photoluminescence spectrum of the monolayer/few-layer/bulk $MoS_2$. Monolayer/few-layer $MoS_2$ by mechanical exfoliation (A) and chemical method (B). Panel A reproduced from Velicky et al. (2016) with permission from American Chemical Society. Panel B reproduced from Eda et al. (2011) with permission from American Chemical Society.

extinction spectroscopy could not only characterize the dispersed nanosheet concentration, but also obtain the detailed information of both the mean nanosheet length and thickness (Varrla et al., 2015). As shown in Fig. 6B, two peaks at ~605 (B-exciton) and ~666 nm (A-exciton) in the optical extinction spectroscopy of single-layer $MoS_2$ are attributed to the direct excitonic transitions at the K point of Brillouin zone. The varying in length (size) and thickness of 2D $MoS_2$ (Fig. 6A) would result in the ratio change of $Ext_B/Ext_{345}$ and the shift of $\lambda_A$ (Fig. 6C and D), respectively.

According to the empirical equation (Backes et al., 2014), the 2D $MoS_2$ thickness could be easily obtained as follows:

$$N_{MoS_2} = 2.3 \times 10^{36} e^{-54{,}888/\lambda_A}$$

where $\lambda_A$, the position of the A-exciton; $N_{MoS_2}$, the layer number of $MoS_2$ nanosheets. $\lambda_A$ as the second derivative of the extinction spectra shows the red-shifting of the peak for thicker nanosheets. The method extremely avoids tedious measurements of nanosheet size and time-consuming statistical microscopic analysis.

### 4.3. Photoluminescence spectrum

Photoluminescence (PL) spectrum is another effective way to qualitatively characterizing the layer number of 2D $MoS_2$ because its PL effect is strongly related to electronic band structure. For example, the photoluminescence of 2D $MoS_2$ synthesized by mechanically exfoliation arises from the intrinsic electronic properties, rather than structural defects or chemical impurities (Eda et al., 2011).

In general, as the increase of layer number, even from monolayer to bilayer shown in Fig. 7A, the PL quantum yield (QY) will dramatically decrease (Wang et al., 2013b). However, the change would be relatively mild for 2D $MoS_2$ synthesized by chemical method (Fig. 7B). Compared with the bulk crystal, the PL QY for the monolayer is increased by more than a factor of $10^4$ (Bertolazzi et al., 2011). Therefore, in essence, the strong photoluminescence effect should be attributed to the direct-to-indirect transition in bandgap due to confinement effects (Scheuschner et al., 2014). In addition to the layer thickness, the lateral dimensions of 2D $MoS_2$ could also affect its PL effect. Because its layer number is not linearly related with the intensity of PL (inset in Fig. 7B), the technique is very useful only for distinguishing the monolayer $MoS_2$ or not (Backes et al., 2014).

## 5. 2D $MoS_2$ used in biosensor fields

The presence of the surface effects and unsaturated d-orbitals contributed by Mo endow 2D $MoS_2$ with a multitude of interesting properties (Wang et al., 2015a; Zeng et al., 2015a). Until now, its applications, including but not limited to, sensors, transistors, integrated circuits, nanometer thick photovoltaics, supercapacitors, and hydrogen evolution catalysis, have demonstrated its unusual versatility (Li et al., 2015, 2014a). In particular, in electronics and optoelectronics fields, such as field effect transistors (FETs), phototransistors, and logic circuits, single layered $MoS_2$ shows a great deal of advantages beyond graphene (zero band gap). Therefore, to some extent, it would be a material complementary to graphene for low-power electronic switching at room temperature. Over the last few years, the burgeoning development in 2D $MoS_2$-based biosensors results from the inherent advantages of 2D $MoS_2$, such as excellent mechanical performance (30 times as strong as steel) (Bertolazzi et al., 2011), exceptional biocompatibility (Xu et al., 2015b), good electrochemical catalyst activity (Wang et al., 2015d), easy modification (Huang et al., 2013a, 2014a; Sun et al., 2014a), high specific surface area and large junction area of the electrode/electrolyte (Zhou et al., 2013), highly efficient fluorescence quenching ability (Xiang et al., 2015; Zhu et al., 2013), high on/off ratios (Radisavljevic et al., 2011), ultrafast saturable absorption (Wang et al., 2013a), and sensitive surface states (high surface-to-volume ratio), as shown in Fig. 2. In particular, high surface-to-volume ratio makes 2D $MoS_2$ particularly sensitive to the changes from its surroundings. On exposure to target analytes, there can be the signal changes in its optical, electronical, and magnetic properties that result from physical and chemical interaction such as absorption, charge transfer and doping, intercalation, and shifts in permittivity and lattice vibrations. Therefore, 2D $MoS_2$ holds great promise for constructing sensors with ultrahigh sensitivity and selectivity. In the following sections, our focus is only put on biosensing applications, in spite of its extensive usefulness in other fields, such as bio-imaging, drug delivery, tissue engineering, and cancer therapy (Chen et al., 2015b; Kalantar-Zadeh et al., 2015; Yang et al., 2015a).

### 5.1. 2D $MoS_2$-based electrochemical biosensors

Benefiting from the rapid developments in nanofabrication and characterization, electrochemical sensors, especially nano-electrochemical sensors, exhibit the greatest potential impact in the areas of healthcare, environmental monitoring (e.g., electronic noses), food packaging (Wei et al., 2009). Such nanoelectrodes can measure ultrafast electron-transfer kinetics that is often too fast to investigate with conventional electrodes (Oja et al., 2013). So far, various nanoscale materials, mainly including noble or transition metals, metal oxides, polymers, organic dyes, biomolecules, ionic liquids, and boronic acid derivatives (Asefa et al., 2009; Gan and Zhao, 2015), have been used to construct nano-electrochemical biosensors. Among them, 2D ultra-thin nanomaterials, even some wide band-gap 2D nanomaterials (Xu et al., 2015a), have attracted a great deal of attention due to their unparalleled advantages in constructing electrochemical biosensors.

It is well-known that the band gap of 2D $MoS_2$ is larger than that of bulk $MoS_2$ and exhibits poor electrical conductivity. Therefore, compared with excellent conductors such as metal and graphene, there seemed to be no advantages for 2D $MoS_2$ in electrochemical biosensors. However, $MoS_2$ nanosheets synthesized by sonication-assisted exfoliation in some solvents (e.g., N, N-dimethylformamide) showed an obviously improved electrocatalytic activity (Wang et al., 2015d). The possible reasons include three aspects. Firstly, the decreasing size and layer number of 2D $MoS_2$ leads to the increasing number of exposed active sites on the edges (out of plane) which possess a much larger heterogeneous electron transfer rate than the basal planes (Chia et al., 2015; Sun et al., 2015, 2014b; Tan et al., 2015). Secondly, 2D $MoS_2$ synthesized by LPE might tend to transfer into a hybrid superlattice of alternating $MoS_2$ monolayers and organic molecules, which would significantly enhance its electrical conductivity due to exotic electrons injections into the inorganic lattice frameworks (Li et al., 2014b; Lin et al., 2013; Wan et al., 2015). In addition, the presence of new surface function groups is also one of important aspects (Wu et al., 2012), because the electrochemical reaction strongly depends on the nature of electrode surfaces (Zhou et al., 2011). However, understanding the mechanism for the improved electro-catalytic activity of 2D $MoS_2$ remains an important and open question.

Up to date, the applications of 2D $MoS_2$ for electrochemical biosensors are in its infancy, which could be mainly divided into two types. The first type is direct electrochemical redox (Wu et al., 2012), that is, 2D $MoS_2$ acts not only as a probe for specifically interacting with the target, but also as an electron transfer mediator or electrochemical catalyst for signal amplification. For

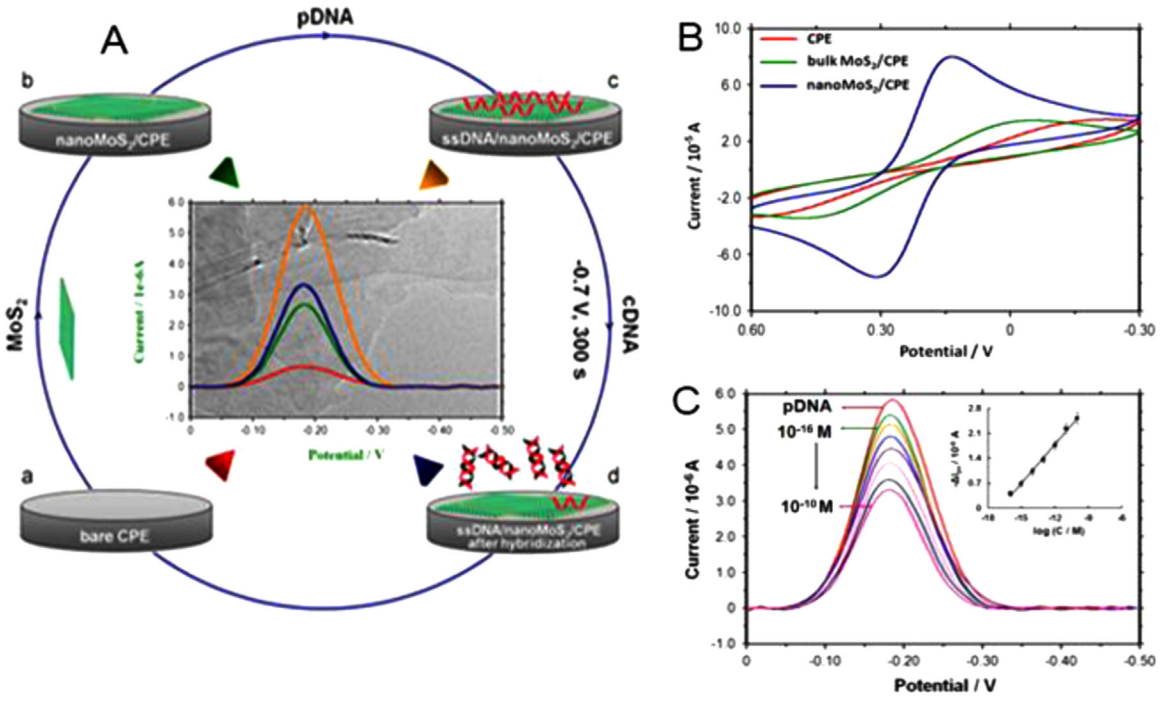


**Fig. 8.** (A) Schematic illustration of the label-free electrochemical DNA assay. (B) CV plots obtained at bare CPE, bulk $MoS_2$/CPE and nano$MoS_2$/CPE in 1.0 M KCl containing 1.0 mM $[Fe(CN)_6]^{3-/4-}$. (C) DPV plots of $2.0 \times 10^{-5}$ M MB at pDNA ($1.0 \times 10^{-6}$ M) modified nano$MoS_2$/CPE and that after hybridization with different concentrations of *tlh* gene sequence. Inset: The plot of $-\Delta I_{pc}$ versus the logarithm of *tlh* gene sequence concentrations. Reproduced from Wang et al. (2015d) with permission from Elsevier B.V.

**Table 1**
2D $MoS_2$-based electrochemical biosensors.

| Electrode | Target | Analytical technique | LOD | Linear wide | Ref. |
|---|---|---|---|---|---|
| GCE-APTES-CS-r$MoS_2$-GOD | Glucose | CV | — | 0–20 mM | (Wu et al., 2012) |
| GCE-APTES-CS-r$MoS_2$ | DA | | | 1–50 μ M | |
| AuNPs@$MoS_2$/GCE | AA, DA,UA | DPV | 50 μM, 50 nM, 50 μM | 50 μM–100 mM, 0.05–30 μM, 50 μM–40 mM | (Sun et al., 2014a) |
| AuNPs@$MoS_2$/GCE | DA | DPV | 80 nM | 0.1–200 mM | (Su et al., 2013) |
| AuNPs/$MoS_2$–PANI/GCE | DA | DPV | 0.1 μM | 1–500 μM | (Huang et al., 2014b) |
| ssDNA/AuNP/GOD/AuNP/$MoS_2$/MWCNT/GCE | DNA | CV | 0.79 fM | 10 fM–10 nM | (Huang et al., 2014d) |
| pDNA/$MoS_2$/CPE | DNA | DPV | 0.019 fM | 0.1 fM-0.1 nM | (Wang et al., 2015d) |
| $MoS_2$–Gr/GCE | AC | DPV | 20 nM | 0.1–100 μM | (Huang et al., 2013b) |
| Ag–$MoS_2$/CS/GCE | Tryptophan | DPV | 0.05 μM | 0.5–120 mM | (Xia et al., 2014) |
| Nafion /Ni–$MoS_2$/GCE | Glucose | AM | 0.31 μM | 0–4 mM | (Huang et al., 2014a) |
| Nafion/Cu–$MoS_2$/GCE | Glucose | AM | — | 0–4 mM | (Huang et al., 2013a) |
| AuNPs/CS–$MoS_2$/GCE | Bisphenol-A | CV | 5 nM | 0.05–100 μM | (Huang et al., 2014c) |
| Laccase/$MoS_2$–GQDs/CSPE | Caffeic acid | CA | 0.32 μM | 0.38–100 μM | (Vasilescu et al., 2016) |
| Nafion–GOD–AuNPs@$MoS_2$/GCE | Glucose | CV | 2.8 μM | 10–200 μM | (Su et al., 2014) |
| $MoS_2$-thionin/GCE | ds DNA | CV | | 0.09–1.9 ng $mL^{-1}$ | (Wang et al., 2014b) |

GCE: glassy carbon electrode; CS: chitosan; APTES: 3-aminopropyltriethoxysilane; r$MoS_2$: reduced $MoS_2$; AA: ascorbic acid; DA: dopamine; UA: uric acid; NPs: nanoparticles; MWCNT: multi-walled carbon nanotube; GOD: glucose oxidase; PANI: polyaniline; ssDNA: single strand DNA; GQDs: graphene quantum dots; CSPE: carbon based screen-printed electrode; CPE: carbon paste electrode; ds DNA: double-stranded DNA; AC: acetaminophen; AM: amperometric measurement; CV: cyclic voltammetry; DPV: differential pulse voltammetry. CA: chronoamperometry.

example, Wang et al. (2015d) synthesized $MoS_2$ nanosheets with high electrochemical activity by ultrasound exfoliation method (Fig. 8B). Taking advantage of its different affinity towards ssDNA versus double-stranded DNA (dsDNA), a label-free ultrasensitive electrochemical DNA sensor was developed (Fig. 8A) and displayed a detection limit as low as 0.019 fM and a linear range of from 0.1 nM–0.1 fM for DNA detection (Fig. 8C). Wu et al. (2012) investigated the electrocatalytic activity of single-layer $MoS_2$ after electrochemical reduction in NaCl aqueous solution by cyclic voltammetry (CV). It was found that the electrochemically reduced $MoS_2$ (r$MoS_2$) exhibited good conductivity and fast electron transfer rate in the $[Fe(CN)_6]^{3-/4-}$ and $[Ru(NH_3)_6]^{2+/3+}$ redox systems. Further, 3-aminopropyltriethoxysilane (APTES), chitosan (CS), and r$MoS_2$ were used to modify glassy carbon electrode (GCE) for obtaining GCE-APTES-CS-r$MoS_2$ to detect dopamine (DA) in the presence of ascorbic acid (AA) and uric acid (UA). The biosensor showed good selectivity with a linear range from 1 to 50 μM.

In general, it is rarely reported that pristine 2D $MoS_2$ was directly applied to construct electrochemical biosensors due to its inherent disadvantages, such as easy aggregation or restacking. Therefore, combining 2D $MoS_2$ with other nanomaterials, in particular nanoscale conductors (Table 1), such as noble metals (e.g., Au (Su et al., 2013; Sun et al., 2014a) and Ag (Xia et al., 2014) nanoparticles), transition metals (e.g., Ni (Huang et al., 2014a) and Cu (Huang et al., 2013a) nanoparticles), carbon materials (e.g., graphene (Huang et al., 2013b), carbon nanotubes (Huang et al.,

2014d), and graphene quantum dots (Vasilescu et al., 2016)), and conductive polymers (e.g., polyaniline (Huang et al., 2014b)), could realize synergetically signal amplification, meanwhile prevent it from aggregation to some extent. These strategies are based on the fact that the combination of two or more different materials to prepare composites could minimize the drawbacks and maximize the advantages of the individual components; more importantly, in addition to the desired performances that could be obtained after the formation of composites, some novel functions might also be generated (Huang et al., 2014e; Zeng et al., 2014). For instance, the specific surface area of 2D $MoS_2$ used as an electrode material will be significantly decreased; however, the synthesis or assembly of 2D $MoS_2$ on, in or with other nanostructures can effectively retain its large specific surface area (Tan and Zhang, 2015). Sun et al. (2014a) synthesized the Au nanoparticles (AuNPs)-decorated $MoS_2$ nanosheets (AuNPs@$MoS_2$) by electrodeposition, which possessed better properties than pure Au NPs or $MoS_2$ nanosheets. The as-formed AuNPs@$MoS_2$ film modified electrode showed excellent electrocatalytic activity towards the oxidation of AA, DA and UA. By chemical reduction, Huang et al. (2013a) first synthesized Cu nanoparticles-decorated $MoS_2$ nanosheets that exhibited synergistic electrocatalytic activity on the oxidation of glucose with a high sensitivity of 1055 μA $mM^{-1}$ $cm^{-2}$ and a linear range up to 4 mM. In the electrochemical biosensors, 2D $MoS_2$ was served not only as a flexible substrate due to its excellent mechanical performance, but also as a good catalyst because of high surface-to-volume ratio.

As for the second type of electrochemical biosensors, 2D $MoS_2$ only plays the role for signal amplification, while the high selectivity or affinity towards the target analytes is obtained with the help of some specific reactions, such as enzyme–substrate interactions, antibody–antigen complexing, and DNA hybridation. For example, Wu et al. (2012) used CV to electrochemically reduce $MoS_2$ nanosheets obtained by Li-intercalated and exfoliation method. The reduced $MoS_2$ ($rMoS_2$) nanosheets showed the improved conductivity and fast electron transfer rate compared with the pristine $MoS_2$ nanosheets. Taking advantage of the specific interaction between glucose oxidase (GOD) and glucose, an electrochemical sensor based on GCE-APTES-CS-$rMoS_2$-GOD for glucose detection was successfully constructed. The biosensor showed a wide linear range from 0 to 20 mM due to the good conductivity and biocompatibility of $rMoS_2$ nanosheets. Wang et al. (2014b) synthesized a layered $MoS_2$–thionin composite by sonicating their mixture in an ionic liquid of 1-butyl-3-methylimidazolium hexafluorophosphate and gradient centrifugation. Based on the intercalation and electrostatic interaction of thionin with DNA, a double-stranded DNA (dsDNA) electrochemical biosensor was developed. The biosensor could be used to detect circulating DNA from healthy human serum even in the presence of relatively high concentration of protein, which exhibited a linear range of from 0.09 to 1.9 ng $mL^{-1}$ and a sensitivity of 0.19 μA mL $ng^{-1}$.

More frequently, 2D $MoS_2$-based electrochemical biosensors were constructed using the two mechanisms at the same time. Huang et al. (2014d) developed an electrochemical DNA sensor by assembling a thiol-tagged DNA probe on a $MoS_2$/multi-walled carbon nanotube (MWCNT) and AuNP-modified GCE that has already been coupled with GOD. Before and after DNA hybridization, the direct electron transfer rate would be accordingly changed due to the spatial blocking, based on which an electrochemical DNA sensor was constructed. Integrating $MoS_2$/MWCNT composites and AuNPs for multiple signal amplification, the biosensor showed a low detection limit of 0.79 fM with a linear range from 10 to $10^7$ fM. Vasilescu et al. (2016) first synthesized a nanocomposite of $MoS_2$ nanoflakes and graphene quantum dots (GQDs) as the compatible matrix for laccase immobilization. The as-formed laccase/$MoS_2$-GQDs modified carbon based screen-printed electrodes showed high selectivity and sensitivity toward caffeic acid due to the high catalytic performance and good biocompatibility of the $MoS_2$-GQDs nanocomposite. The biosensor exhibited a linear range of 0.38–100 μM, a detection limit of 0.32 μM and a sensitivity of 17.92 nA $mM^{-1}$.

### 5.2. 2D $MoS_2$-based fluorescent biosensors

In theory, 2D $MoS_2$-based fluorescent biosensors should be divided into two types. The first type is using 2D $MoS_2$ as efficient quenchers by fluorescence resonance energy transfer (FRET) (Ping et al., 2015). The second type is based on the intrinsic fluorescence emission of 2D $MoS_2$ itself, rather than the labeled fluorophores. Take the latter as an example, the photoluminescent emission strongly depends on its layer number, lateral dimension or size, and the surface nature (Kalantar-Zadeh et al., 2015; Li et al., 2015; Zhang et al., 2013). Therefore, the high fluorescent emission is usually obtained by taking advantage of decreasing dimension or size, or doping to tune the electron band structure (Liu et al., 2015a; Splendiani et al., 2010). As the recognition events occur between 2D $MoS_2$ or 2D $MoS_2$-based composites and target analytes, the fluorescent of nanomaterials might decrease or disappear, based on which fluorescent biosensors are constructed.

Up to now, most of 2D $MoS_2$-based fluorescent biosensors belong to the former. Therefore, the following discussion would only focus on the fluorescent biosensors using 2D $MoS_2$ as excellent nanoquenchers by forming a Förster (or fluorescence) resonance energy transfer pair (Zhang et al., 2015d), in which the distance-dependent fluorescence quenching is closely coupled with the recognition events. In this process, the photoexcitation energy is transferred from a donor fluorophore to an acceptor molecule based on the spectral overlap between the emission of donor and

**Table 2**
2D $MoS_2$-based fluorescent biosensors.

| Materials | Target | Signal amplification mechanism (The main role of 2D $MoS_2$) | LOD | Linear wide | Ref. |
|---|---|---|---|---|---|
| ssDNA- $MoS_2$ | ssDNA<br>Adenosine | Fluorescence quenching ability | 500 pM<br>5 μM | 0–15 nM<br>— | (Zhu et al., 2013) |
| FITC-ssDNA-$MoS_2$ | $Ag^+$ | Fluorescence quenching ability | 1 nM | 1–100 nM | (Mao et al., 2015) |
| DNAzyme-$MoS_2$ | $UO_2^{2+}$ | Fluorescence quenching ability | 2.14 nM | 0–100 nM | (Zhang et al., 2015a) |
| Exo III-TPSMLD-$MoS_2$ | Streptavidin | Fluorescence quenching ability | 0.67 ng $ml^{-1}$ | 0–600 ng $mL^{-1}$ | (Xiang et al., 2015) |
| TA-$MoS_2$/rGO | Glutathione | Photocatalysis performance | 25.0 μM | 60–700 mM | (Zhang et al., 2015b) |
| $MoS_2$–RhoBS | $Ag^+$ in aqueous solution and *E. coli* bacteria | Fluorescence quenching ability and catalytic reduction performance | 10 nM | 10–500 nM | (Yang et al., 2015b) |

ssDNA: single strand DNA; FITC: fluorescein isothiocyanate; Exo III: exonuclease III; TPSMLD: terminal protection of small-molecule-linked DNA; TA: terephthalic acid; rGO: graphene oxide. RhoBS: rhodamine B isothiocyanate. Of note, the detection environment of target usually refers to aqueous solution without specific notation.

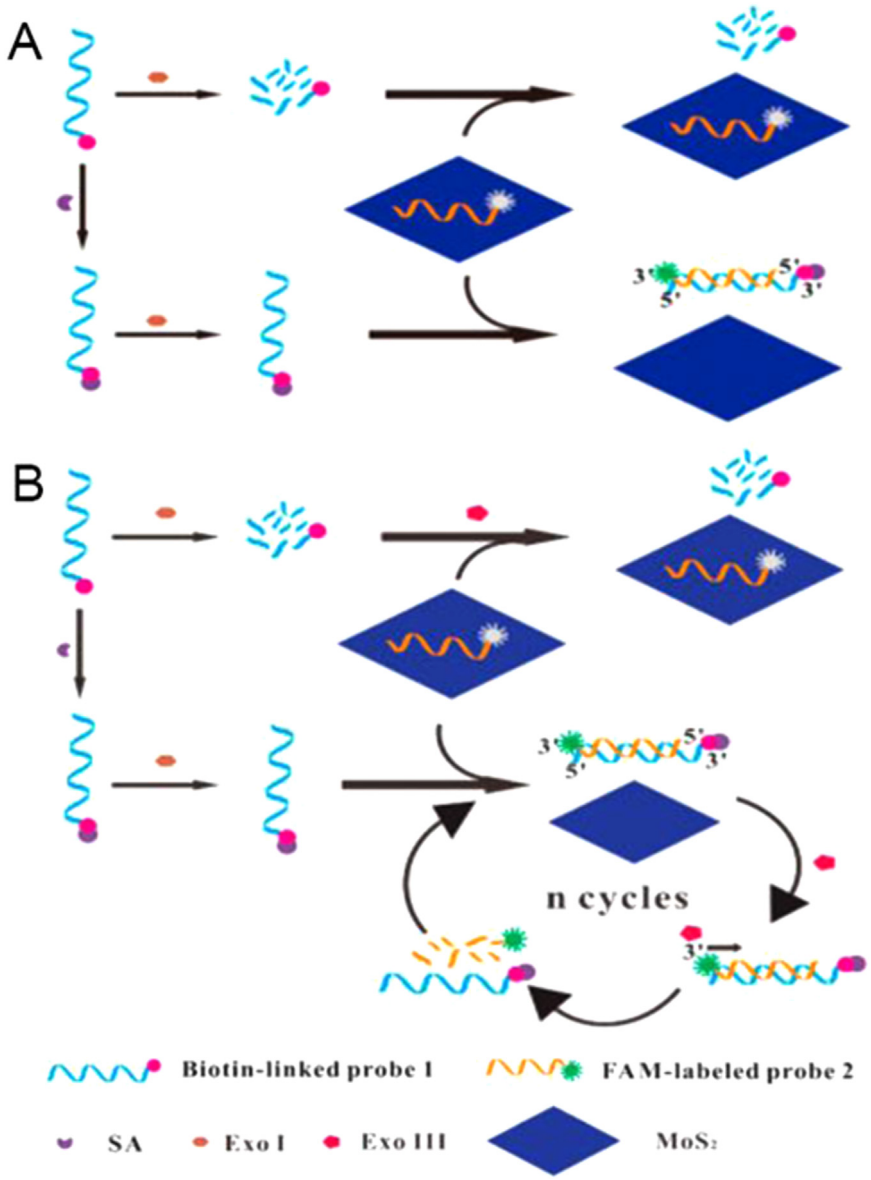


**Fig. 9.** Scheme of the mechanism of a $MoS_2$-based biosensor for SA detection via TPSMLD (A) and a $MoS_2$-based biosensor for SA detection via TPSMLD and Exo III-aided DNA recycling amplification (B). Reproduced from Xiang et al. (2015) with permission from 2013 Elsevier B.V.

the absorbance of acceptor. In general, fluorescence quenching between donor (e.g., dye molecules) and acceptor (e.g., 2D $MoS_2$) involves two major mechanisms including energy transfer through dipole–dipole interactions and electron/charge transfer. Thereinto, the dipole–dipole interaction is achieved through space by the overlap of dipolar electric fields between donor and acceptor. Regarding the latter, the interaction is made through the overlap of the orbitals of donor and acceptor (Tan et al., 2013).

Considering good biocompatibility, large surface areas, highly efficient fluorescence quenching ability of 2D $MoS_2$ for signal amplification, many 2D $MoS_2$-based fluorescent biosensors have been developed. A typical example is that Zhang group (Zhang et al., 2015d; Zhu et al., 2013) first used $MoS_2$ nanosheets by electrochemical lithium-intercalation method to construct fluorogenic nanoprobes for detecting DNA and small molecules. Initially, no fluorescence signal could be observed due to the highly efficient fluorescence quenching ability of $MoS_2$ nanosheets towards dye-labeled single-stranded DNA (ssDNA) probe immobilized via the van der Waals force. After the ssDNA probe was hybridized with its complementary target DNA, the fluorescence signal could be recovery because the interaction between the formed double-stranded DNA (dsDNA) and $MoS_2$ nanosheets became weak. The strong but different fluorescence quenching abilities towards dye-labeled ssDNA versus dsDNA endows the DNA biosensor with high selectivity and sensitivity. Its detection limit and linear range are 500 pM ($3\sigma$) and from 0 to 15 nM, respectively. In addition, another biosensor has been developed by anti-adenosine aptamer probe modified $MoS_2$ nanosheets. The biosensor showed a detection limit of 5 μM ($3\sigma$) for adenosine detection.

Based on the pioneering work, various $MoS_2$ nanosheet-based fluorescent biosensors have been constructed, as shown in Table 2. Mao et al. (2015) took advantage of high fluorescence quenching efficiency of $MoS_2$ nanosheets for signal amplification. In this process, two oligonucleotides (one labeled with FITC) with C–C mismatches to form stable C–$Ag^+$–C base pairs for high selectivity to $Ag^+$. The biosensor showed a linear range from 1 to 100 nM, and the detection limit of 1 nM ($3\sigma$). Xiang et al. (2015) reported a new $MoS_2$ nanosheet-based fluorescent biosensor for protein detection by terminal protection of small-molecule-linked DNA

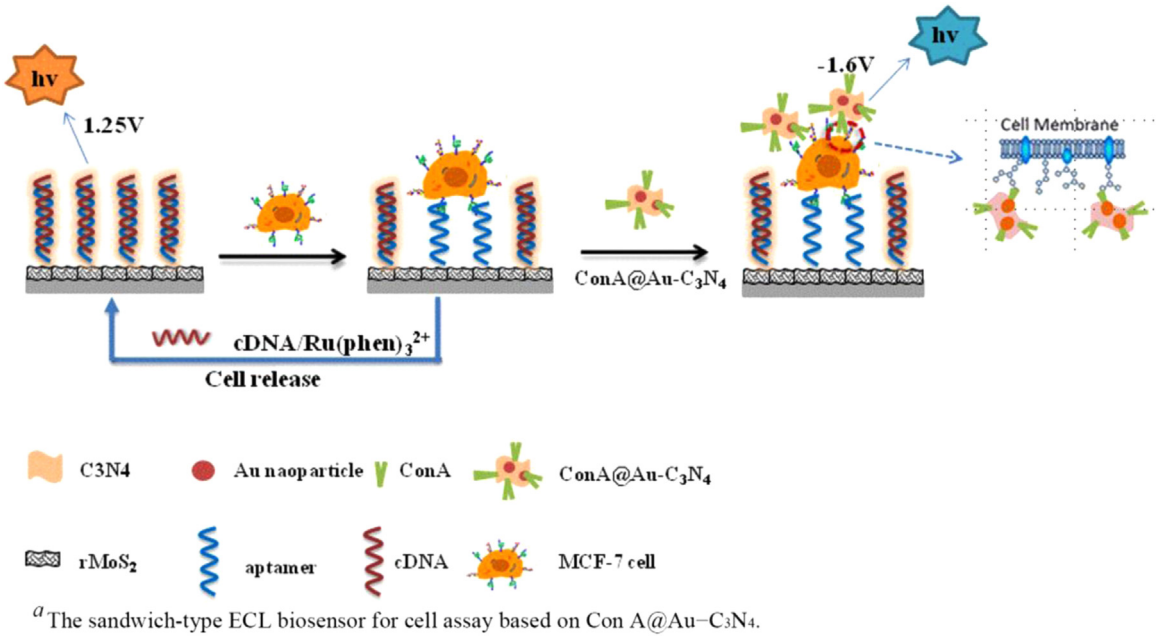


[a] The sandwich-type ECL biosensor for cell assay based on Con A@Au−C$_3$N$_4$.

**Fig. 10.** Schematic illustration of ECL biosensor for carbohydrate expression on cell surface [a]. Reproduced from He et al. (2015) with permission from American Chemical Society.

(TPSMLD) and exonuclease III-aided DNA recycling amplification. Taking SA-biotin system as a model, the strong and specific binding of SA to the small molecule biotin of probe DNA (probe 1) avoided the degradation by Exo I. As a result, the fluorescence signal could be recovered by the hybridization between the probe 1 and probe 2 (AFM-ssDNA, the complementary sequence of probe 1) (Fig. 9A). Accordingly, the presence of protein SA was related to the concentration of residual probe 1. Exonuclease III-aided DNA recycling amplification significantly improved the sensitivity of the biosensor which exhibited a detection limit of 0.67 ng mL$^{-1}$ SA (Fig. 9B).

### 5.3. 2D $MoS_2$-based electrochemiluminescence (ECL) biosensors

Electrochemiluminescence (ECL) is a combination of electrochemical and chemiluminescent methods. It involves a light emission process in a redox reaction of electrogenerated reactants at electrode surfaces (He et al., 2015; Liu et al., 2015b; Richter, 2004). In 2D $MoS_2$-based ECL biosensors, 2D $MoS_2$ itself could not produce electrochemiluminescence, but plays other roles, such as acting as a robust substrate or for signal amplification. In contrast, ECL signal is generated through other nanomaterials such as quantum dots or quantum dots coated with polymers. For example, He et al. (2015) used the excellent electrochemical properties and the large surface of $MoS_2$ nanosheets to improve the electron transfer rate and enhance the cell capture efficiency on the electrode interface. Meanwhile, concanavalin A (Con A) conjugated gold nanoparticle-modified graphite–$C_3N_4$ (Con A@Au–g–$C_3N_4$) as a negative ECL nanoprobe was applied for the cell surface N-glycan evaluation due to the excellent ECL properties of g-$C_3N_4$ at negative potential. The ECL signal intensity at positive potential were associated with the numbers of the cells that competitively adsorbed on the electrode (Fig. 10). On the other hand, the changes at negative potential were related to both the numbers of the cells and their surface glycans. Therefore, the ratio of the ECL signal intensity of negative potential *versus* that of positive potential ($\Delta ECL_{neg}/\Delta ECL_{pos}$) could be a parameter for accurately and directly exhibiting N-glycan expression. The as-formed ECL cytosensor displayed excellent performances for the analysis of the MCF-7 cancer cell and its surface N-glycan evaluation in human serum samples. Similarly, other ECL sensors have been constructed by combing 2D $MoS_2$ with one type (e.g. Au, (Liu et al., 2014c; Wang et al., 2015c) CdS (Shi et al., 2015a) ) or a few types (e.g., CdSe–chitosan (Ke et al., 2015), graphene–Au (Liu et al., 2014d)) of nanomaterials for signal amplification by synergistic effects.

### 5.4. 2D $MoS_2$-based colorimetric biosensor

So far, a few 2D $MoS_2$-based colorimetric biosensors have been reported, which are mainly based on the intrinsic peroxidase-like activity of 2D $MoS_2$ (Lin et al., 2014; Nirala et al., 2015). Lin et al. (2014) first reported its intrinsic peroxidase-like activity can catalytically oxidize 3, 3', 5, 5'-tetramethylbenzidine (TMB) by $H_2O_2$ to produce a color reaction (a typical deep-blue color) (Fig. 11A). In this process, $MoS_2$ nanosheets could facilitate the electron transfer between TMB and $H_2O_2$, and catalyze the decomposition of $H_2O_2$ in acidic media into ·OH. Based on this phenomenon, a highly sensitive and selective colorimetric method for $H_2O_2$ and glucose detection was developed by using the $MoS_2$ nanosheets-TMB-$H_2O_2$ system. The biosensors exhibited a linear range from 5 to 100 mmol L$^{-1}$ with a detection limit of 1.5 mmol L$^{-1}$ for $H_2O_2$ detection (Fig. 11B and C), a linear range from 5 to 150 mmol L$^{-1}$ with a limit of detection of 1.2 mmol L$^{-1}$ for glucose detection in serum samples (Fig. 11D and E), respectively. In addition, Nirala et al. (2015) took advantage of the peroxidase like activity of both $MoS_2$ nanoribbons and Au nanoparticles for synergistically enhanced colorimetric detection of cholesterol. The proposed $MoS_2$ NRs–Au NPs system could realize quick and reliable detection of free cholesterol using unaided eye with a linear range from 0.04 to 1 mM and a detection limit of 0.015 mM.

### 5.5. 2D $MoS_2$-based field-effect transistor (FET) biosensors

Feld-effect transistor (FET) electronic biosensors offer a simple, real-time, efficient, and low-cost sensing platform for a variety of target analytes, because of rapid electrical detection without labeling the biomolecules, low power consumption, portability, inexpensive mass production, and the possibility of on-chip

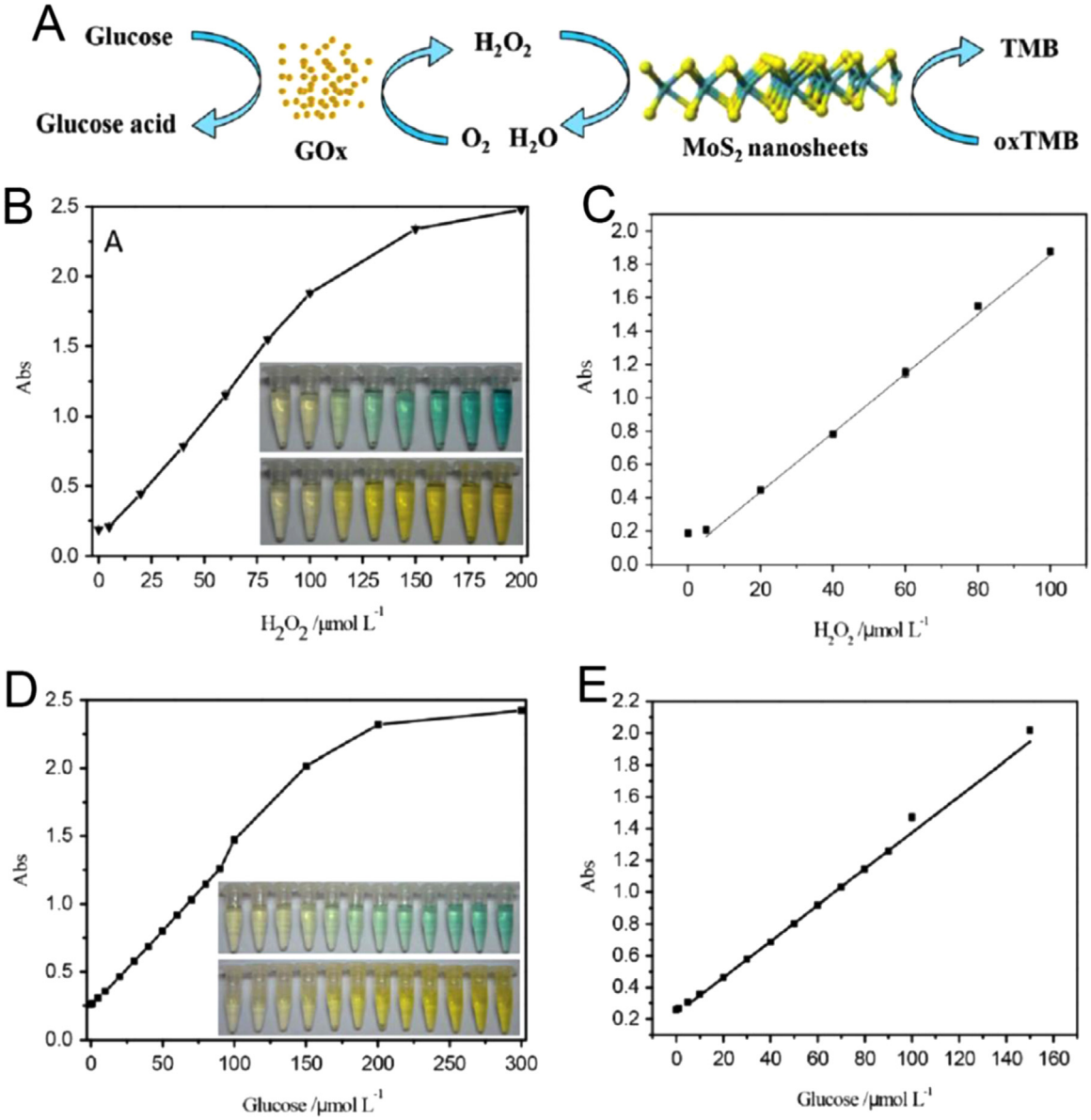


**Fig. 11.** (A) Schematic illustration of colorimetric detection of glucose by using glucose oxidase ($GO_x$) and $MoS_2$ nanosheet-catalyzed reactions. (B) A dose–response curve for $H_2O_2$ detection and (C) the linear calibration plot for $H_2O_2$. The inset of (B) are images of colored products for different concentrations of $H_2O_2$ before (top) and after (down) adding of 10 mL 20% (v/v) sulfuric acid. (D) A dose–response curve for glucose detection and (E) the linear calibration plot for glucose. The inset of (D) are the images of colored products for different concentrations of glucose before (top) and after (down) the addition of 10 mL 20% (v/v) sulfuric acid. Reproduced from Lin et al. (2014) with permission from Royal Society of Chemistry. (For interpretation of the references to color in this figure legend, the reader is referred to the web version of this article.)

integration of both sensor and measurement systems (Kalantar-Zadeh et al., 2015; Late et al., 2013; Nam et al., 2015; Sarkar et al., 2014; Wang et al., 2014a; Yoon et al., 2011). Various device geometries have been reported, including 1D nanomaterials, and 2D layered nanomaterials (e.g., graphene (Mohanty and Berry, 2008) and $MoS_2$ (Lee et al., 2014)). Compared with FET biosensors based on 2D nanomaterials, it is rather difficult for 1D nanostructures to construct low-cost, scalable, and reliable FET biosensors due to the constraints of nanofabrication (Lee et al., 2009). As such, FET biosensors based on 2D nanomaterials have been extensively studied for detecting various of targets such as protein (Lee et al., 2014) and DNA (Lee et al., 2015) because 2D nanomaterials could offer a large sensing area for high responsivity (Cheng et al., 2013), ease of fabrication (Kim et al., 2013), low noise level in solution (Cheng et al., 2010), and high sensitivity to biomolecules (Dong et al., 2010; Ohno et al., 2009).

In contrast to graphene with zero band gap, 2D $MoS_2$, in particular, a single-layer (SL) $MoS_2$ nanosheet, is a semiconductor with a direct band gap which could significantly lower the leakage current and allow remarkable on/off ratios ( $> 10^8$) with acceptable carrier mobility, low subthreshold swing (SS, ~70 mV per decade), and ultralow standby power dissipation (Radisavljevic et al., 2011). Moreover, 2D $MoS_2$ shows ultrafast saturable absorption (Wang et al., 2013a) and tends to interact strongly with donor-like targets, which have unique potential for the gas detection such as triethylamine, ammonia, and NO (Friedman et al., 2014; Perkins et al., 2013). Generally, 2D $MoS_2$-based FET biosensors show the n-type behavior; the existence of a band gap would significantly improve its sensitivity (Lee et al., 2015). The detection mechanism of FET electronic biosensors, as shown in Fig. 12A, is based on a conductivity change in response to variations in the electric field or potential at the surface, because the carrier density is sensitive to the change of the electric field in a direction perpendicular to the gate surface (Matsumoto and Miyahara, 2013).

Sarkar et al. (2014) reported a $MoS_2$-based FET biosensor using

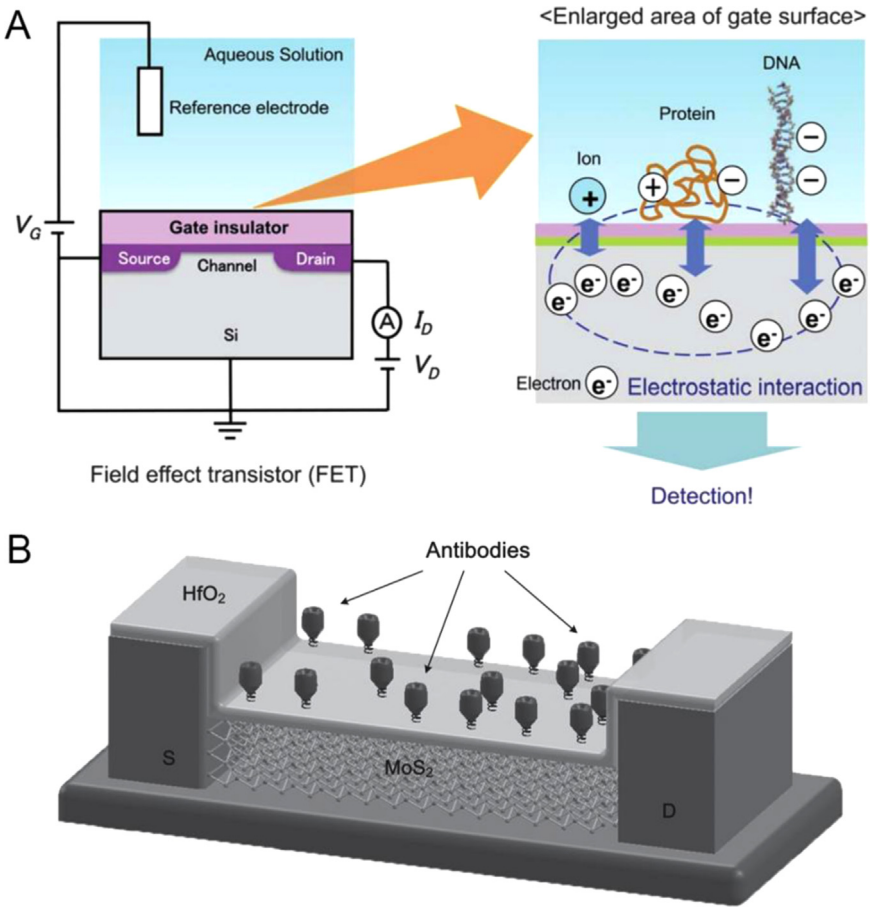


**Fig. 12.** (A) Structure and principles of field effect transistor based bio-sensing. Schematic diagram of $MoS_2$-based FET biosensor. Reproduced from Matsumoto and Miyahara (2013) with permission from Royal Society of Chemistry. (B) Schematic of the biofunctionalization layers on the device surface (S: source, D: drain). Reproduced from Wang et al. (2014a) with permission from John Wiley & Sons Publishing Company.

biotin modified 2D $MoS_2$ as gate material for streptavidin detection. Its sensitivity as high as 196 could be obtained in the subthreshold region for a streptavidin solution of 100 fM even with a very thick dielectric layer such as 2D $MoS_2$ with four atomic layers. Monolayer $MoS_2$-based FET biosensor showed a higher sensitivity and lower detection of limit due to relatively large surface-to-volume ratio, but it would also result in unstable response (Li et al., 2012a). Given this situation, Wang et al. (2014a) first reported label-free and real-time detection of prostate-specific antigens (PSA) based on multi-layer $MoS_2$ nanosheet-based field-effect device (Fig. 12B). The as-formed biosensor showed high sensitivity as low as sub-picomolar ranges and excellent selectivity due to the specific binding of PSA and antibody. The introduction of dielectric environment for multi-layer $MoS_2$ could improve the sensitivity (Kim et al., 2012). In addition, some alternative strategies such as synthesizing $MoS_2$-based hybrid materials (He et al., 2012), surface functionalization (Kim et al., 2014), and using monolayer $MoS_2$ prepared by CVD (Perkins et al., 2013), were extensively applied to improve the performances of 2D $MoS_2$-based FET biosensors.

## 6. Conclusions and future perspectives

In this review, we mainly discussed the synthesis and characteristic methods of 2D $MoS_2$, the relationships between structure and property, recent advances of 2D $MoS_2$-based biosensors. In general $MoS_2$-based biosensors are in their infancy, even though the rapid development occurred in 2D $MoS_2$-based electrochemical, fluorescent, and FET biosensors in the past few years. A grand challenge for 2D $MoS_2$-based biosensors is to develop cost-effective, sensitive, and selective methods for detecting target analytes. Essentially, it could be ascribed to the control, high-quality, and large scale synthesis of atomically thin and uniform 2D $MoS_2$, either in solution or on substrates, for further constructing desirable material architectures, and deeply understanding about surface or interface process of the recognition events.

From a long-term view, various van der Waals heterostructures (stacking the 2D materials on top of each other), offers an array of possibilities to broaden the applicability of 2D materials, because van der Waals could act as a versatile 'glue' to engineer the structure and properties. Especially, 2D TMD monolayers can have an optical bandgap in the near-infrared to visible spectral range and exhibit extremely strong light-matter interactions due to quantum-well transitions, which could expand the 2D material family in novel optoelectronic devices (Azizi et al., 2015; Caldwell and Novoselov, 2015; Cho et al., 2015; He et al., 2014; Hong et al., 2014; Wang and Xia, 2015). Some van der Waals heterostructures could realize ultrafast charge transfer and high efficient photocurrent (Hong et al., 2014). Furthermore, the bottom-up synthesis of the heterostructures do not require the stringent lattice-matching requirements (Jena and Konar, 2007). Therefore, $MoS_2$-based photoelectrochemical biosensors using van der Waals heterostructures as the building blocks would be a promising but new field. In general, one point for sure is that 2D $MoS_2$ and other graphene analogs of layered materials will still play important roles in biosensor fields. To functionalize or tailor 2D $MoS_2$ would offer more flexible design room for constructing the probes and

improving the sensing performances.

## Acknowledgements

This study was supported by National Natural Science Foundation of China (No. 21477012).

## References

Asefa, T., Duncan, C.T., Sharma, K.K., 2009. Analyst 134, 1980–1990.
Ataca, C., Şahin, H., Ciraci, S., 2012. J. Phys. Chem. C 116, 8983–8999.
Azizi, A., Eichfeld, S., Geschwind, G., Zhang, K., Jiang, B., Mukherjee, D., Hossain, L., Piasecki, A.F., Kabius, B., Robinson, J.A., Alem, N., 2015. ACS Nano 9, 4882–4890.
Backes, C., Smith, R.J., McEvoy, N., Berner, N.C., McCloskey, D., Nerl, H.C., O'Neill, A., King, P.J., Higgins, T., Hanlon, D., Scheuschner, N., Maultzsch, J., Houben, L., Duesberg, J.N., Donegan, J.F., Nicolosi, V., Coleman, J.N., 2014. Nat. Commun. 5, 4576. http://dx.doi.org/10.1038/ncomms5576.
Bertolazzi, S., Brivio, J., Kis, A., 2011. ACS Nano 5, 9703–9709.
Butler, S.Z., Hollen, S.M., Cao, L.Y., Cui, Y., Gupta, J.A., Gutierrez, H.R., Heinz, T.F., Hong, S.S., Huang, J.X., Ismach, A.F., Johnston-Halperin, E., Kuno, M., Plashnitsa, V.V., Robinson, R.D., Ruoff, R.S., Salahuddin, S., Shan, J., Shi, L., Spencer, M.G., Terrones, M., Windl, W., Goldberger, J.E., 2013. ACS Nano 7, 2898–2926.
Caldwell, J.D., Novoselov, K.S., 2015. Nat. Mater. 14, 364–366.
Castellanos-Gomez, A., Barkelid, M., Goossens, A.M., Calado, V.E., van der Zant, H.S. J., Steele, G.A., 2012. Nano Lett. 12, 3187–3192.
Cha, J.J., Koski, K.J., Huang, K.C., Wang, K.X., Luo, W., Kong, D., Yu, Z., Fan, S., Brongersma, M.L., Cui, Y., 2013. Nano Lett. 13, 5913–5918.
Chakraborty, B., Bera, A., Muthu, D.V.S., Bhowmick, S., Waghmare, U.V., Sood, A.K., 2012. Phys. Rev. B 85, 161403. http://dx.doi.org/10.1103/PhysRevB.85.161403.
Chakraborty, B., Matte, H.S.S.R., Sood, A.K., Rao, C.N.R., 2013. J. Raman Spectrosc. 44, 92–96.
Chen, F., Xia, J.L., Ferry, D.K., Tao, N.J., 2009. Nano Lett. 9, 2571–2574.
Chen, S.Y., Zheng, C., Fuhrer, M.S., Yan, J., 2015a. Nano Lett. 15, 2526–2532.
Chen, Y., Tan, C., Zhang, H., Wang, L., 2015b. Chem. Soc. Rev. 44, 2681–2701.
Cheng, Z.G., Hou, J.F., Zhou, Q.Y., Li, T.Y., Li, H.B., Yang, L., Jiang, K.L., Wang, C., Li, Y.C., Fang, Y., 2013. Nano Lett. 13, 2902–2907.
Cheng, Z.G., Li, Q., Li, Z.J., Zhou, Q.Y., Fang, Y., 2010. Nano Lett. 10, 1864–1868.
Chhowalla, M., Shin, H.S., Eda, G., Li, L.J., Loh, K.P., Zhang, H., 2013. Nat. Chem. 5, 263–275.
Chia, X., Eng, A.Y., Ambrosi, A., Tan, S.M., Pumera, M., 2015. Chem. Rev. 115, 11941–11966.
Cho, B., Yoon, J., Lim, S.K., Kim, A.R., Kim, D.H., Park, S.G., Kwon, J.D., Lee, Y.J., Lee, K. H., Lee, B.H., Ko, H.C., Hahm, M.G., 2015. ACS Appl. Mater. Interfaces 7, 16775–16780.
Choudhary, N., Park, J., Hwang, J.Y., Choi, W., 2014. ACS Appl. Mater. Interfaces 6, 21215–21222.
Coleman, J.N., Lotya, M., O'Neill, A., Bergin, S.D., King, P.J., Khan, U., Young, K., Gaucher, A., De, S., Smith, R.J., Shvets, I.V., Arora, S.K., Stanton, G., Kim, H.Y., Lee, K., Kim, G.T., Duesberg, G.S., Hallam, T., Boland, J.J., Wang, J.J., Donegan, J.F., Grunlan, J.C., Moriarty, G., Shmeliov, A., Nicholls, R.J., Perkins, J.M., Grieveson, E. M., Theuwissen, K., McComb, D.W., Nellist, P.D., Nicolosi, V., 2011. Science 331, 568–571.
Colson, J.W., Woll, A.R., Mukherjee, A., Levendorf, M.P., Spitler, E.L., Shields, V.B., Spencer, M.G., Park, J., Dichtel, W.R., 2011. Science 332, 228–231.
Cunningham, G., Lotya, M., Cucinotta, C.S., Sanvito, S., Bergin, S.D., Menzel, R., Shaffer, M.S.P., Coleman, J.N., 2012. ACS Nano 6, 3468–3480.
Del Corro, E., Terrones, H., Elias, A., Fantini, C., Feng, S.M., Nguyen, M.A., Mallouk, T. E., Terrones, M., Pimenta, M.A., 2014. ACS Nano 8, 9629–9635.
Dong, X.C., Shi, Y.M., Huang, W., Chen, P., Li, L.J., 2010. Adv. Mater. 22, 1649–1653.
Eda, G., Yamaguchi, H., Voiry, D., Fujita, T., Chen, M., Chhowalla, M., 2011. Nano Lett. 11, 5111–5116.
Friedman, A.L., Keith Perkins, F., Cobas, E., Jernigan, G.G., Campbell, P.M., Hanbicki, A.T., Jonker, B.T., 2014. Solid-State Electron. 101, 2–7.
Gan, X.R., Zhao, H.M., 2015. Sens. Mater. 27, 191–215.
Ganatra, R., Zhang, Q., 2014. ASC Nano 8, 4074–4099.
Gao, G., Jiao, Y., Ma, F., Jiao, Y., Waclawik, E., Du, A., 2015. J. Phys. Chem. C 119, 13124–13128.
Geim, A.K., Grigorieva, I.V., 2013. Nature 499, 419–425.
Ghatak, S., Pal, A.N., Ghosh, A., 2011. ACS Nano 5, 7707–7712.
Gołasa, K., Grzeszczyk, M., Leszczyński, P., Faugeras, C., Nicolet, A.A.L., Wysmołek, A., Potemski, M., Babiński, A., 2014. Appl. Phys. Lett. 104, 092106. http://dx.doi.org/10.1063/1.4867502.
Guan, G., Zhang, S., Liu, S., Cai, Y., Low, M., Teng, C.P., Phang, I.Y., Cheng, Y., Duei, K.L., Srinivasan, B.M., Zheng, Y., Zhang, Y.W., Han, M.Y., 2015. J. Am. Chem. Soc. 137, 6152–6155.
Guo, Y.Q., Xu, K., Wu, C.Z., Zhao, J.Y., Xie, Y., 2015. Chem. Soc. Rev. 44, 637–646.
Gupta, A., Sakthivel, T., Seal, S., 2015. Prog. Mater. Sci. 73, 44–126.
He, J., Kumar, N., Bellus, M.Z., Chiu, H.Y., He, D., Wang, Y., Zhao, H., 2014. Nat. Commun. 5, 5622. http://dx.doi.org/10.1038/ncomms6622.
He, Q., Zeng, Z., Yin, Z., Li, H., Wu, S., Huang, X., Zhang, H., 2012. Small 8, 2994–2999.
He, Y., Li, J., Liu, Y., 2015. Anal. Chem. 87, 9777–9785.
Heine, T., 2015. Acc. Chem. Res. 48, 65–72.
Hong, X., Kim, J., Shi, S.F., Zhang, Y., Jin, C., Sun, Y., Tongay, S., Wu, J., Zhang, Y., Wang, F., 2014. Nat. Nanotechnol. 9, 682–686.
Houssa, M., Dimoulas, A., Molle, A., 2015. J. Phys. Condens. Matter. 27, 253002. http://dx.doi.org/10.1088/0953-8984/27/25/253002.
Huang, J., Dong, Z., Li, Y., Li, J., Tang, W., Yang, H., Wang, J., Bao, Y., Jin, J., Li, R., 2013a. Mater. Res. Bull. 48, 4544–4547.
Huang, J., He, Y., Jin, J., Li, Y., Dong, Z., Li, R., 2014a. Electrochim. Acta 136, 41–46.
Huang, K.J., Wang, L., Li, J., Liu, Y.M., 2013b. Sens. Actuators B: Chem 178, 671–677.
Huang, K.J., Zhang, J.Z., Liu, Y.J., Wang, L.L., 2014b. Sens. Actuators B: Chem 194, 303–310.
Huang, K.J., Liu, Y.J., Liu, Y.M., Wang, L.L., 2014c. J. Hazard. Mater 276, 207–215.
Huang, K.J., Liu, Y.J., Wang, H.B., Wang, Y.Y., Liu, Y.M., 2014d. Biosens. Bioelectron. 55, 195–202.
Huang, X., Tan, C., Yin, Z., Zhang, H., 2014e. Adv. Mater. 26, 2185–2204.
Huang, X., Tang, S., Mu, X., Dai, Y., Chen, G., Zhou, Z., Ruan, F., Yang, Z., Zheng, N., 2011. Nat. Nanotechnol. 6, 28–32.
Huang, X., Zeng, Z., Zhang, H., 2013c. Chem. Soc. Rev. 42, 1934–1946.
Huang, Y.H., Peng, C.C., Chen, R.S., Huang, Y.S., Ho, C.H., 2014f. Appl. Phys. Lett., 105. http://dx.doi.org/10.1063/1.4894857.
Jena, D., Konar, A., 2007. Phys. Rev. Lett., 98. http://dx.doi.org/10.1103/PhysRevLett.98.136805.
Jeong, S., Yoo, D., Jang, J.T., Kim, M., Cheon, J., 2012. J. Am. Chem. Soc. 134, 18233–18236.
Ji, Q., Zhang, Y., Gao, T., Zhang, Y., Ma, D., Liu, M., Chen, Y., Qiao, X., Tan, P.H., Kan, M., Feng, J., Sun, Q., Liu, Z., 2013. Nano Lett. 13, 3870–3877.
Jia, L., Ding, L., Tian, J., Bao, L., Hu, Y., Ju, H., Yu, J.S., 2015. Nanoscale 7, 15953–15961.
Jiang, S., Arguilla, M.Q., Cultrara, N.D., Goldberger, J.E., 2015. Acc. Chem. Res. 48, 144–151.
Kalantar-zadeh, K., Ou, J.Z., 2016. ACS Sens. 1, 5–16.
Kalantar-zadeh, K., Ou, J.Z., Daeneke, T., Strano, M.S., Pumera, M., Gras, S.L., 2015. Adv. Funct. Mater. 25, 5086–5099.
Kannan, P.K., Late, D.J., Morgan, H., Rout, C.S., 2015. Nanoscale 7, 13293–13312.
Kaul, A.B., 2014. J. Mater. Res. 29, 348–361.
Ke, R., Zhang, X., Wang, L., Zhang, C., Zhang, S., Niu, H., Mao, C., Song, J., Jin, B., Tian, Y., 2015. J. Solid State Electrochem. 19, 1633–1641.
Kim, D.J., Sohn, I.Y., Jung, J.H., Yoon, O.J., Lee, N.E., Park, J.S., 2013. Biosens. Bioelectron. 41, 621–626.
Kim, J.S., Yoo, H.W., Choi, H.O., Jung, H.T., 2014. Nano Lett. 14, 5941–5947.
Kim, S., Konar, A., Hwang, W.S., Lee, J.H., Lee, J., Yang, J., Jung, C., Kim, H., Yoo, J.B., Choi, J.Y., Jin, Y.W., Lee, S.Y., Jena, D., Choi, W., Kim, K., 2012. Nat. Commun. 3, 1–7.
Kory, M.J., Worle, M., Weber, T., Payamyar, P., van de Poll, S.W., Dshemuchadse, J., Trapp, N., Schluter, A.D., 2014. Nat. Chem. 6, 779–784.
Kou, L., Chen, C., Smith, S.C., 2015. J. Phys. Chem. Lett. 6, 2794–2805.
Kuc, A., Heine, T., 2015. Chem. Soc. Rev. 44, 2603–2614.
Kuc, A., Zibouche, N., Heine, T., 2011. Phys. Rev. B, 83. http://dx.doi.org/10.1103/PhysRevB.83.245213.
Late, D.J., Huang, Y.K., Liu, B., Acharya, J., Shirodkar, S.N., Luo, J.J., Yan, A.M., Charles, D., Waghmare, U.V., Dravid, V.P., Rao, C.N.R., 2013. ACS Nano 7, 4879–4891.
Lee, C., Yan, H., Brus, L.E., Heinz, T.F., Hone, J., Ryu, S., 2010. ACS Nano 4, 2695–2700.
Lee, D.W., Lee, J., Sohn, I.Y., Kim, B.Y., Son, Y.M., Bark, H., Jung, J., Choi, M., Kim, T.H., Lee, C., Lee, N.E., 2015. Nano Res. 8, 2340–2350.
Lee, J., Dak, P., Lee, Y., Park, H., Choi, W., Alam, M.A., Kim, S., 2014. Sci. Rep., 4. http://dx.doi.org/10.1038/srep07352.
Lee, K., Nair, P.R., Scott, A., Alam, M.A., Janes, D.B., 2009. J. Appl. Phys. 105 (102046), 13.
Li, B.L., Zou, H.L., Lu, L., Yang, Y., Lei, J.L., Luo, H.Q., Li, N.B., 2015. Adv. Funct. Mater. 25, 3541–3550.
Li, H., Wu, J., Yin, Z., Zhang, H., 2014a. Acc. Chem. Res. 47, 1067–1075.
Li, H., Yin, Z., He, Q., Li, H., Huang, X., Lu, G., Fam, D.W., Tok, A.I., Zhang, Q., Zhang, H., 2012a. Small 8, 63–67.
Li, H., Zhang, Q., Yap, C.C.R., Tay, B.K., Edwin, T.H.T., Olivier, A., Baillargeat, D., 2012b. Adv. Funct. Mater. 22, 1385–1390.
Li, T., Liu, Y.H., Chitara, B., Goldberger, J.E., 2014b. J. Am. Chem. Soc. 136, 2986–2989.
Li, X., Zhu, H., 2015. J. Materiom. 1, 33–44.
Lin, C., Zhu, X., Feng, J., Wu, C., Hu, S., Peng, J., Guo, Y., Peng, L., Zhao, J., Huang, J., Yang, J., Xie, Y., 2013. J. Am. Chem. Soc. 135, 5144–5151.
Lin, T., Zhong, L., Guo, L., Fu, F., Chen, G., 2014. Nanoscale 6, 11856–11862.
Liu, B.L., Chen, L., Liu, G., Abbas, A.N., Fathi, M., Zhou, C.W., 2014a. ACS Nano 8, 5304–5314.
Liu, N., Kim, P., Kim, J.H., Ye, J.H., Kim, S., Lee, C.J., 2014b. ACS Nano 8, 6902–6910.
Liu, X.J., Li, L.P., Wei, Y.J., Zheng, Y.Z., Xiao, Q., Feng, B., 2015a. Analyst 140, 4654–4661.
Liu, Y.M., Zhou, M., Liu, Y.Y., Shi, G.F., Zhang, J.J., Cao, J.T., Huang, K.J., Chen, Y.H., 2014c. RSC Adv. 4, 22888–22893.
Liu, Y.L., Nan, H.Y., Wu, X., Pan, W., Wang, W.H., Bai, J., Zhao, W.W., Sun, L.T., Wang, X.R., Ni, Z.H., 2013. ACS Nano 7, 4202–4209.
Liu, Y.M., Zhou, M., Liu, Y.Y., Huang, K.J., Cao, J.T., Zhang, J.J., Shi, G.F., Chen, Y.H., 2014d. Anal. Methods 6, 4152–4157.
Liu, Z., Qi, W., Xu, G., 2015b. Chem. Soc. Rev. 44, 3117–3142.
Lu, P., Wu, X., Guo, W., Zeng, X.C., 2012. Phys. Chem. Chem. Phys. 14, 13035–13040.
Lv, R., Robinson, J.A., Schaak, R.E., Sun, D., Sun, Y.F., Mallouk, T.E., Terrones, M., 2015. Acc. Chem. Res. 48, 56–64.
Mahjouri-Samani, M., Lin, M.W., Wang, K., Lupini, A.R., Lee, J., Basile, L., Boulesbaa,

A., Rouleau, C.M., Puretzky, A.A., Ivanov, I.N., Xiao, K., Yoon, M., Geohegan, D.B., 2015. Nat. Commun. 6, 7749. http://dx.doi.org/10.1038/ncomms8749.
Mak, K.F., Lee, C., Hone, J., Shan, J., Heinz, T.F., 2010. Phys. Rev. Lett., 105. http://dx.doi.org/10.1103/PhysRevLett.105.136805.
Mao, K., Wu, Z., Chen, Y., Zhou, X., Shen, A., Hu, J., 2015. Talanta 132, 658–663.
Matsumoto, A., Miyahara, Y., 2013. Nanoscale 5, 10702–10718.
McCreary, K.M., Hanbicki, A.T., Robinson, J.T., Cobas, E., Culbertson, J.C., Friedman, A. L., Jernigan, G.G., Jonker, B.T., 2014. Adv. Funct. Mater. 24, 6449–6454.
Mohanty, N., Berry, V., 2008. Nano Lett. 8, 4469–4476.
Molina-Sánchez, A., Wirtz, L., 2011. Phys. Rev. B, 84.
Naguib, M., Gogotsi, Y., 2015. Acc. Chem. Res. 48, 128–135.
Najmaei, S., Yuan, J., Zhang, J., Ajayan, P., Lou, J., 2015. Acc. Chem. Res. 48, 31–40.
Nam, H., Oh, B.-R., Chen, P., Yoon, J.S., Wi, S., Chen, M., Kurabayashi, K., Liang, X., 2015. Appl. Phys. Lett. 107, 012105. http://dx.doi.org/10.1063/1.4926800.
Nicolosi, V., Chhowalla, M., Kanatzidis, M.G., Strano, M.S., Coleman, J.N., 2013. Science 340, 1420–1438.
Nirala, N.R., Pandey, S., Bansal, A., Singh, V.K., Mukherjee, B., Saxena, P.S., Srivastava, A., 2015. Biosens. Bioelectron. 74, 207–213.
Niu, T., Li, A., 2015. Prog. Surf. Sci. 90, 21–45.
Novoselov, K.S., Fal'ko, V.I., Colombo, L., Gellert, P.R., Schwab, M.G., Kim, K., 2012. Nature 490, 192–200.
Novoselov, K.S., Geim, A.K., Morozov, S.V., Jiang, D., Zhang, Y., Dubonos, S.V., Grigorieva, I.V., Firsov, A.A., 2004. Science 306, 666–669.
Novoselov, K.S., Jiang, D., Schedin, F., Booth, T.J., Khotkevich, V.V., Morozov, S.V., Geim, A.K., 2005. Proc. Natl. Acad. Sci. USA 102, 10451–10453.
Ohno, Y., Maehashi, K., Yamashiro, Y., Matsumoto, K., 2009. Nano Lett. 9, 3318–3322.
Oja, S.M., Wood, M., Zhang, B., 2013. Anal. Chem. 85, 473–486.
Pan, Y., Zhang, L., Huang, L., Li, L., Meng, L., Gao, M., Huan, Q., Lin, X., Wang, Y., Du, S., Freund, H.J., Gao, H.J., 2014. Small 10, 2215–2225.
Peng, Y., Li, Y.S., Ban, Y.J., Jin, H., Jiao, W.M., Liu, X.L., Yang, W.S., 2014. Science 346, 1356–1359.
Perkins, F.K., Friedman, A.L., Cobas, E., Campbell, P.M., Jernigan, G.G., Jonker, B.T., 2013. Nano Lett. 13, 668–673.
Perumal Veeramalai, C., Li, F., Xu, H., Kim, T.W., Guo, T., 2015. RSC Adv. 5, 57666–57670.
Pimenta, M.A., Del Corro, E., Carvalho, B.R., Fantini, C., Malard, L.M., 2015. Acc. Chem. Res. 48, 41–47.
Ping, J.F., Zhou, Y.B., Wu, Y.Y., Papper, V., Boujday, S., Marks, R.S., Steele, T.W.J., 2015. Biosens. Bioelectron. 64, 373–385.
Pisoni, A., Jacimovic, J., Barisic, O.S., Walter, A., Nafradi, B., Bugnon, P., Magrez, A., Berger, H., Revay, Z., Forro, L., 2015. J. Phys. Chem. C 119, 3918–3922.
Prabhakar Vattikuti, S.V., Byon, C., Venkata Reddy, C., Venkatesh, B., Shim, J., 2015. J. Mater. Sci. 50, 5024–5038.
Radisavljevic, B., Kis, A., 2013. Nat. Mater. 12, 815–820.
Radisavljevic, B., Radenovic, A., Brivio, J., Giacometti, V., Kis, A., 2011. Nat. Nanotechnol. 6, 147–150.
Ramakrishna Matte, H.S.S., Gomathi, A., Manna, A.K., Late, D.J., Datta, R., Pati, S.K., Rao, C.N.R., 2010. Angew. Chem. Int. Ed. 122, 4153–4156.
Richter, M.M., 2004. Chem. Rev. 104, 3003–3036.
Robinson, B. J., Giusca, C. E., Gonzalez, Y. T., Kay, N. D., Kazakova, O., Kolosov, O.V., 2015. 2D Materials 2, 015005.
Sandoval, S.J., Yang, D., Frindt, R.F., Irwin, J.C., 1991. Phys. Rev. B 44, 3955–3962.
Sarkar, D., Liu, W., Xie, X.J., Anselmo, A.C., Mitragotri, S., Banerjee, K., 2014. ACS Nano 8, 3992–4003.
Scheuschner, N., Ochedowski, O., Kaulitz, A.M., Gillen, R., Schleberger, M., Maultzsch, J., 2014. Phys. Rev. B, 89. http://dx.doi.org/10.1103/PhysRevB.89.125406.
Shen, J., He, Y., Wu, J., Gao, C., Keyshar, K., Zhang, X., Yang, Y., Ye, M., Vajtai, R., Lou, J., Ajayan, P.M., 2015. Nano Lett. 15, 5449–5454.
Shi, G.F., Cao, J.T., Zhang, J.J., Liu, Y.M., Chen, Y.H., Ren, S.W., 2015a. Sens. Actuators B: Chem. 220, 340–346.
Shi, J., Yang, Y., Zhang, Y., Ma, D., Wei, W., Ji, Q., Zhang, Y., Song, X., Gao, T., Li, C., Bao, X., Liu, Z., Fu, Q., Zhang, Y., 2015b. Adv. Funct. Mater. 25, 842–849.
Shi, Y., Li, H., Li, L.J., 2015c. Chem. Soc. Rev. 44, 2744–2756.
Shi, Y.M., Zhou, W., Lu, A.Y., Fang, W.J., Lee, Y.H., Hsu, A.L., Kim, S.M., Kim, K.K., Yang, H.Y., Li, L.J., Idrobo, J.C., Kong, J., 2012. Nano Lett. 12, 2784–2791.
Smith, R.J., King, P.J., Lotya, M., Wirtz, C., Khan, U., De, S., O'Neill, A., Duesberg, G.S., Grunlan, J.C., Moriarty, G., Chen, J., Wang, J., Minett, A.I., Nicolosi, V., Coleman, J. N., 2011. Adv. Mater. 23, 3944–3948.
Splendiani, A., Sun, L., Zhang, Y., Li, T., Kim, J., Chim, C.Y., Galli, G., Wang, F., 2010. Nano Lett. 10, 1271–1275.
Su, S., Chao, J., Pan, D., Wang, L., Fan, C., 2015. Electroanalysis 27, 1062–1072.
Su, S., Sun, H.F., Xu, F., Yuwen, L.H., Fan, C.H., Wang, L.H., 2014. Microchim. Acta 181, 1497–1503.
Su, S., Sun, H.F., Xu, F., Yuwen, L.H., Wang, L.H., 2013. Electroanalysis 25, 2523–2529.
Sun, H., Chao, J., Zuo, X., Su, S., Liu, X., Yuwen, L., Fan, C., Wang, L., 2014a. RSC Adv. 4, 27625–27629.
Sun, Y., Gao, S., Lei, F., Xie, Y., 2015. Chem. Soc. Rev. 44, 623–636.
Sun, Y., Gao, S., Xie, Y., 2014b. Chem. Soc. Rev. 43, 530–546.
Tan, A.T., Kim, J., Huang, J.K., Li, L.J., Huang, J., 2013. Small 9, 3253–3258.
Tan, C., Zhang, H., 2015. Chem. Soc. Rev. 44, 2713–2731.
Tan, S.M., Ambrosi, A., Sofer, Z., Huber, S., Sedmidubsky, D., Pumera, M., 2015. Chem. Eur. J 21, 7170–7178.
Tang, Q., Zhou, Z., 2013. Prog. Mater. Sci. 58, 1244–1315.
Tonndorf, P., Schmidt, R., Bottger, P., Zhang, X., Borner, J., Liebig, A., Albrecht, M., Kloc, C., Gordan, O., Zahn, D.R.T., de Vasconcellos, S.M., Bratschitsch, R., 2013. Opt. Express. 21, 4908–4916.
Varrla, E., Backes, C., Paton, K.R., Harvey, A., Gholamvand, Z., McCauley, J., Coleman, J.N., 2015. Chem. Mater. 27, 1129–1139.
Vasilescu, I., Eremia, S.A.V., Kusko, M., Radoi, A., Vasile, E., Radu, G.L., 2016. Biosens. Bioelectron. 75, 232–237.
Veeramalai, C.P., Li, F.S., Xu, H.Y., Kim, T.W., Guo, T.L., 2015. RSC Adv. 5, 57666–57670.
Velicky, M., Bissett, M.A., Woods, C.R., Toth, P.S., Georgiou, T., Kinloch, I.A., Novoselov, K.S., Dryfe, R.A., 2016. Nano Lett. . http://dx.doi.org/10.1021/acs.nanolett.5b05317
Vogel, E.M., Robinson, J.A., 2015. MRS Bull. 40, 558–563.
Wan, C., Gu, X., Dang, F., Itoh, T., Wang, Y., Sasaki, H., Kondo, M., Koga, K., Yabuki, K., Snyder, G.J., Yang, R., Koumoto, K., 2015. Nat. Mater. 14, 622–627.
Wang, H., Yuan, H., Sae Hong, S., Li, Y., Cui, Y., 2015a. Chem. Soc. Rev. 44, 2664–2680.
Wang, K.P., Wang, J., Fan, J.T., Lotya, M., O'Neill, A., Fox, D., Feng, Y.Y., Zhang, X.Y., Jiang, B.X., Zhao, Q.Z., Zhang, H.Z., Coleman, J.N., Zhang, L., Blau, W.J., 2013b. ACS Nano 7, 9260–9267.
Wang, L., Wang, Y., Wong, J.I., Palacios, T., Kong, J., Yang, H.Y., 2014a. Small 10, 1101–1105.
Wang, Q.H., Kalantar-Zadeh, K., Kis, A., Coleman, J.N., Strano, M.S., 2012. Nat. Nanotechnol. 7, 699–712.
Wang, T.Y., Zhu, R.Z., Zhuo, J.Q., Zhu, Z.W., Shao, Y.H., Li, M.X., 2014b. Anal. Chem. 86, 12064–12069.
Wang, W., Li, L., Wu, K., Zhu, G., Tan, S., Li, W., Yang, Y., 2015b. RSC Adv. 5, 61799–61807.
Wang, X., Deng, W., Shen, L., Yan, M., Ge, S., Yu, J., 2015c. New J. Chem. 39, 8100–8107.
Wang, X., Nan, F., Zhao, J., Yang, T., Ge, T., Jiao, K., 2015d. Biosens. Bioelectron. 64, 386–391.
Wang, X., Xia, F., 2015. Nat. Mater. 14, 264–265.
Wang, Y.C., Ou, J.Z., Balendhran, S., Chrimes, A.F., Mortazavi, M., Yao, D.D., Field, M. R., Latham, K., Bansal, V., Friend, J.R., Zhuiykov, S., Medhekar, N.V., Strano, M.S., Kalantar-zadeh, K., 2013b. ACS Nano 7, 10083–10093.
Wang, Z., Chen, T., Chen, W., Chang, K., Ma, L., Huang, G., Chen, D., Lee, J.Y., 2013c. J. Mater. Chem. A 1, 2202–2210.
Wei, D., Bailey, M.J., Andrew, P., Ryhanen, T., 2009. Lab Chip 9, 2123–2131.
Wu, S., Zeng, Z., He, Q., Wang, Z., Wang, S.J., Du, Y., Yin, Z., Sun, X., Chen, W., Zhang, H., 2012. Small 8, 2264–2270.
Xia, X., Zheng, Z., Zhang, Y., Zhao, X., Wang, C., 2014. Sens. Actuators B: Chem. 192, 42–50.
Xiang, X., Shi, J., Huang, F., Zheng, M., Deng, Q., Xu, J., 2015. Biosens. Bioelectron. 74, 227–232.
Xu, Q., Cai, L., Zhao, H., Tang, J., Shen, Y., Hu, X., Zeng, H., 2015a. Biosens. Bioelectron. 63, 294–300.
Xu, S., Li, D., Wu, P., 2015b. Adv. Funct. Mater. 25, 1127–1136.
Yang, D., Sandoval, S.J., Divigalpitiya, W.M.R., Irwin, J.C., Frindt, R.F., 1991. Phys. Rev. B 43, 12053–12056.
Yang, G., Zhu, C., Du, D., Zhu, J., Lin, Y., 2015a. Nanoscale 7, 14217–14231.
Yang, Y., Liu, T., Cheng, L., Song, G.S., Liu, Z., Chen, M.W., 2015b. ACS Appl. Mater. Interfaces 7, 7526–7533.
Yoon, Y., Ganapathi, K., Salahuddin, S., 2011. Nano Lett. 11, 3768–3773.
Yu, X.Y., Hu, H., Wang, Y., Chen, H., Lou, X.W., 2015. Angew. Chem. Int. Ed. 54, 7395–7398.
Zeng, H.L., Zhu, B.R., Liu, K., Fan, J.H., Cui, X.D., Zhang, Q.M., 2012. Phys. Rev. B, 86. http://dx.doi.org/10.1103/PhysRevB.86.241301.
Zeng, Q., Wang, H., Fu, W., Gong, Y., Zhou, W., Ajayan, P.M., Lou, J., Liu, Z., 2015. Small 11, 1868–1884.
Zeng, Q.S., Wang, H., Fu, W., Gong, Y.J., Zhou, W., Ajayan, P.M., Lou, J., Liu, Z., 2015b. Small 11, 1868–1884.
Zeng, Z., Tan, C., Huang, X., Bao, S., Zhang, H., 2014. Energy Environ. Sci. 7, 797–803.
Zeng, Z., Yin, Z., Huang, X., Li, H., He, Q., Lu, G., Boey, F., Zhang, H., 2011. Angew. Chem. Int. Ed. 50, 11093–11097.
Zhang, H., 2015. ACS Nano . http://dx.doi.org/10.1021/acsnano.5b05040.
Zhang, H.Y., Ruan, Y.J., Lin, L., Lin, M.G., Zeng, X.X., Xi, Z.M., Fu, F.F., 2015a. Spectrochim. Acta A 146, 1–6.
Zhang, J., Yu, H., Chen, W., Tian, X.Z., Liu, D.H., Cheng, M., Xie, G.B., Yang, W., Yang, R., Bai, X.D., Shi, D.X., Zhang, G.Y., 2014a. ACS Nano 8, 6024–6030.
Zhang, N., Ma, W., Han, D., Wang, L., Wu, T., Niu, L., 2015b. Talanta 144, 551–558.
Zhang, W., Huang, J.K., Chen, C.H., Chang, Y.H., Cheng, Y.J., Li, L.J., 2013. Adv. Mater. 25, 3456–3461.
Zhang, W., Zhang, P., Su, Z., Wei, G., 2015c. Nanoscale 7, 18364–18378.
Zhang, Y., Ji, Q.Q., Han, G.F., Ju, J., Shi, J.P., Ma, D.L., Sun, J.Y., Zhang, Y.S., Li, M.J., Lang, X.Y., Zhang, Y.F., Liu, Z.F., 2014b. ACS Nano 8, 8617–8624.
Zhang, Y., Zheng, B., Zhu, C.F., Zhang, X., Tan, C.L., Li, H., Chen, B., Yang, J., Chen, J.Z., Huang, Y., Wang, L.H., Zhang, H., 2015d. Adv. Mater. 27, 935–939.
Zhao, W., Ribeiro, R.M., Eda, G., 2015. Acc. Chem. Res. 48, 91–99.
Zhao, Y., Luo, X., Li, H., Zhang, J., Araujo, P.T., Gan, C.K., Wu, J., Zhang, H., Quek, S.Y., Dresselhaus, M.S., Xiong, Q., 2013. Nano Lett. 13, 1007–1015.
Zhou, M., Lou, X.W., Xie, Y., 2013. Nano Today 8, 598–618.
Zhou, Z.Y., Tian, N., Li, J.T., Broadwell, I., Sun, S.G., 2011. Chem. Soc. Rev. 40, 4167–4185.
Zhu, C., Zeng, Z., Li, H., Li, F., Fan, C., Zhang, H., 2013. J. Am. Chem. Soc. 135, 5998–6001.
Zhuang, X.D., Mai, Y.Y., Wu, D.Q., Zhang, F., Feng, X.L., 2015. Adv. Mater. 27, 403–427.